Genetic and pharmacological reduction of CDK14 mitigates synucleinopathy

Maxime W C Rousseaux

max.rousseaux@uottawa.ca

   University of Ottawa

Jean-Louis Parmasad
   University of Ottawa   https://orcid.org/0000-0001-5013-2317

Konrad Ricke
   University of Ottawa

Morgan Stykel
   University of Guelph

Brodie Buchner-Duby
   University of Guelph

Benjamin Nguyen
   University of Ottawa

Amanda Bruce
   University of Ottawa

Haley Geertsma
   University of Ottawa

Eric Lian
   Ottawa Hospital Research Institute

Nathalie Lengacher
   Ottawa Hospital Research Institute   https://orcid.org/0000-0002-2536-1895

Steve Callaghan
   University of Ottawa

Alvin Joselin
   University of Calgary   https://orcid.org/0000-0002-9010-0421

Julianna Tomlinson
   Ottawa Hospital Research Institute

Michael Schlossmacher
   Ottawa Hospital Research Institute

William Stanford

Sprott Centre for Stem Cell Research, Ottawa Hospital Research Institute, 501 Smyth Road, Ottawa, Ontario K1L8L6, Canada   https://orcid.org/0000-0002-5813-8016

Jiyan Ma

Van Andel Institute

Patrik Brundin

Van Andel Research Institute   https://orcid.org/0000-0003-2924-5186

Scott Ryan

The University of Guelph, Canada

Article

Additional Declarations: (Not answered)

Genetic and pharmacological reduction of CDK14 mitigates α-synuclein pathology in human neurons and in rodent models of Parkinson's disease

Authors: Jean-Louis A. Parmasad[1,2,†], Konrad M. Ricke[1,2,3†], Morgan G. Stykel[4], Brodie Buchner-Duby[4], Benjamin Nguyen[1,2,3], Amanda Bruce[1,2], Haley M. Geertsma[1,2,3], Eric Lian[5,6], Nathalie A. Lengacher[1,3,5], Steve M. Callaghan[1,2,3], Alvin Joselin[7], Julianna J. Tomlinson[1,3,5], Michael G. Schlossmacher[1,3,5], William L. Stanford[2,5,6], Jiyan Ma[8,#], Patrik Brundin[8], Scott D. Ryan[4], and Maxime W.C. Rousseaux[1,2,3,6,*]

Affiliations:

[1] University of Ottawa Brain and Mind Research Institute, Ottawa, ON

[2] Department of Cellular and Molecular Medicine, University of Ottawa, Ottawa, ON

[3] Aligning Science Across Parkinson's (ASAP) Collaborative Research Network, Chevy Chase, MD

[4] Department of Molecular and Cellular Biology, University of Guelph, Guelph, ON

[5] Program in Neuroscience, Ottawa Hospital Research Institute, Ottawa, ON

[6] Ottawa Institute for Systems Biology, University of Ottawa, Ottawa, ON

[7] Hotchkiss Brain Institute, Department of Clinical Neurosciences, University of Calgary, Calgary, AB

[8] Parkinson's Disease Center, Department of Neurodegenerative Science, Van Andel Institute, Grand Rapids, MI

[†]Authors contributed equally

[#]Present address: Chinese Institute for Brain Research, Beijing, China

*Corresponding author. Email: max.rousseaux@uottawa.ca

Abstract:

Parkinson's disease (PD) is a debilitating neurodegenerative disease characterized by the loss of midbrain dopaminergic neurons (DaNs) and the abnormal accumulation of α-Synuclein (α-Syn) protein. Currently, no treatment can slow nor halt the progression of PD. Multiplications and mutations of the α-Syn gene (*SNCA*) cause PD-associated syndromes and animal models that overexpress α-Syn replicate several features of PD. Decreasing total α-Syn levels, therefore, is an attractive approach to slow down neurodegeneration in patients with synucleinopathy. We previously performed a genetic screen for modifiers of α-Syn levels and identified CDK14, a kinase of largely unknown function as a regulator of α-Syn. To test the potential therapeutic effects of CDK14 reduction in PD, we ablated Cdk14 in the α-Syn preformed fibrils (PFF)-induced PD mouse model. We found that loss of Cdk14 mitigates the grip strength deficit of PFF-treated mice and ameliorates PFF-induced cortical α-Syn pathology, indicated by reduced numbers of pS129 α-Syn-containing cells. In primary neurons, we found that Cdk14 depletion protects against the propagation of toxic α-Syn species. We further validated these findings on pS129 α-Syn levels in PD patient neurons. Finally, we leveraged the recent discovery of a covalent inhibitor of CDK14 to determine whether this target is pharmacologically tractable *in vitro* and *in vivo*. We found that CDK14 inhibition decreases total and pathologically aggregated α-Syn in human neurons, in PFF-challenged rat neurons and in the brains of α-Syn-humanized mice. In summary, we suggest that CDK14 represents a novel therapeutic target for PD-associated synucleinopathy.

Keywords: α-Synuclein, Parkinson's disease, Cyclin-dependent kinase 14, Neurodegeneration, Therapeutics

2

INTRODUCTION

Parkinson's disease (PD) is a neurodegenerative disease that affects over 10 million individuals worldwide (1,2). Individuals with PD present with motor symptoms such as bradykinesia, rigidity, shuffling gait, and resting tremor, as well as non-motor symptoms such as constipation, anosmia and sleep disturbances (3–5). Neuropathologically, PD is characterized by the loss of dopaminergic neurons (DaNs) in the *substantia nigra pars compacta* (SN), as well as the accumulation of α-synuclein (α-Syn) containing inclusions, termed Lewy bodies and Lewy neurites (collectively: Lewy pathology) in surviving neurons (6–8). Current treatments address motor deficits, but are less effective on non-motor aspects of the disease and cannot slow down nor halt neurodegeneration in PD (9). Therefore, identifying new 'druggable' targets for PD is clearly warranted. In addition to being abundantly present in Lewy pathology, point mutations and multiplications in the gene encoding α-Syn, *SNCA*, underlie monogenic variants of PD (10,11). Increased levels of *SNCA* mRNA are also observed in laser-captured SN DaNs from PD patients (12), and animal models that overexpress α-Syn replicate several features of PD (13–15). Thus, there is a clear link between increased α-Syn dosage and PD pathogenesis, highlighting the crucial role of α-Syn in the manifestation of PD (16–19).

Since α-Syn dosage is linked to PD, decreasing total α-Syn levels may be a feasible approach to mitigate neurodegeneration in PD patients, regardless of whether oligomeric or fibrillar α-Syn is the toxic culprit. *Snca*-knockout (KO) mice are viable and fertile but display mild cognitive impairments, suggesting that a modest amount of cerebral α-Syn is required to accomplish its physiological role in the synapse (20,21). Titration of excessive α-Syn levels in a non-invasive manner would thus be beneficial in treating a chronic neurodegenerative disease like PD. Specifically, an orally available drug capable of mitigating α-Syn toxicity could offer a

3

78 minimally invasive approach, a feature particularly important in treating a chronic illness. A

79 pooled RNA interference screen investigating 'druggable' modifiers of α-Syn levels identified

80 cyclin-dependent kinase 14 (CDK14, a.k.a. PFTK1; Cdk14 or Pftk1 in mice) as a regulator of α-

81 Syn (22). CDK14 is a brain-expressed protein kinase with a largely unknown biological function

82 (23). Its expression is upregulated in certain cancers, such as esophageal and colorectal cancer, for

83 which it has generated attention as a therapeutic target (24,25). In fact, this has led to the recent

84 development of FMF-04-159-2, a potent, covalent inhibitor of CDK14 (26).

85 Since decreasing CDK14 leads to a mild reduction in endogenous α-Syn levels (22), we

86 hypothesize that genetic and pharmacological inhibition of CDK14 reduces α-Syn pathology and

87 PD-like phenotypes in mice and human cells. To test this hypothesis, we examined the

88 consequence of *Cdk14* reduction on PD-like features in the preformed α-Syn fibrils (PFFs)-

89 induced PD mouse model. We further explored the role of CDK14 in mediating α-Syn spread in

90 primary neurons. We also tested the effect of CRISPR/Cas9-mediated reduction of *CDK14* in

91 human neurons carrying the PD-linked *SNCA* A53T mutation. Lastly, using the covalent CDK14

92 inhibitor, we investigated if pharmacological inhibition of CDK14 is sufficient to decrease α-Syn

93 levels in rodent and human neurons. In summary, we show that decreasing CDK14, both

94 genetically and pharmacologically, reduces α-Syn accumulation, spread, and modifies α-Syn

95 aggregation.

96

97 **MATERIALS AND METHODS**

98 **Mouse strains**

99 *Cdk14*^{+/-} mice were generated by the Gene Targeting and Transgenic Facility of Texas A&M

100 Institute for Genomic Medicine (TIGM), on a mixed (129/SvEvBrd x C57BL/6) background (as

4

described previously (27). *Cdk14*^{+/-} mice were backcrossed 14 times to the C57Bl/6NCrl

background prior to experimentation. *Cdk14*^{+/-} mice were paired to generate *Cdk14*^{-/-} mice. *PAC*

α-Syn[A53T] *TG* founder mice (dbl-PAC-Tg(*SNCA*[A53T])[+/+];*Snca*^{-/-}, (28)) were provided by Robert L.

Nussbaum (University of California, San Francisco, USA). Mice were genotyped using genomic

DNA extracted from ear or tail tissue (genotyping protocol available upon request).

Stereotactic PFF injections

Endotoxin-free recombinant mouse α-Syn fibril preparations were stored at -80 ºC before usage

(29,30). On the day of the stereotactic injections, fibrils were thawed and sonicated in a sonicator

water bath to generate PFFs (Covaris S220, 18 W peak incident power, 20 % duty factor, 50 cycles

per burst, 150 seconds). For transmission electron microscopy (TEM) analysis 0.2 mg/mL PFF

samples were stained with Uranyl Acetate and imaged on an FEI Tecnai G2 Spirit Twin TEM

(Centre for Advanced Materials Research [CAMaR], University of Ottawa). 6-month-old mice

were deeply anesthetized with isoflurane, and 1 µL PFFs (5 mg/mL) or sterile saline (0.9 % NaCl)

was unilaterally delivered into the dorsal striatum of the right hemisphere at these coordinates

relative to bregma: -2 mm medial-lateral; +0.2 mm antero-posterior and -2.6 mm dorso-ventral.

Injections were performed using a 2 µL syringe (Hamilton Company, Reno, NV, USA) at a rate

of 0.1 µL/minute (min) with the needle left in place for at least 3 min before its slow withdrawal.

After surgery, animals were monitored, and post-surgical care was provided. Behavioral

experiments were performed 6 months post-injection, followed by the collection of the brains at 7

months post-injection.

Intracerebroventricular administration of the CDK14 inhibitor FMF-04-159-2

124   Alzet® Mini-Osmotic Pumps (model 2004) were loaded with FMF-04-159-216 (R&D Systems

125   7158, Minneapolis, MN, USA) 1.47 µg/uL in vehicle solution containing 8 % DMSO (Fisher

126   Scientific, BP231, Hampton, NH, USA), 2 % Tween 80 (Fisher Scientific, BP338-500) and 90 %

127   ddH$_2$O) 16 hours before stereotactic surgeries. Brain infusion catheters with 3.5 cm long catheter

128   tubing (Alzet® Brain Infusion Kit) were attached as per manufacturer's instructions. Brain

129   infusion assemblies were incubated at 37 °C in sterile saline until implantation. 4-month-old *PAC*

130   *α-Syn*^{A53T} *TG* were deeply anesthetized with isoflurane for the stereotactic implantation of brain

131   infusion assemblies. FMF-04-159-2 (release rate of 0.35 mg/kg/day) or its vehicle solution was

132   continuously administered into the cerebral ventricles (coordinates relative to bregma: -1.1 mm

133   medial-lateral; -0.5 mm antero-posterior and -3 mm dorso-ventral) for 28 days with the brain

134   infusion catheter attached to the skull and the connected pump in a subcutaneous pocket of the

135   mouse's back. The body weight of mice was measured and their activity, neurological signs, facial

136   grimace, coat condition and respiration were scored (from 0 to 3) within 28 days after the surgery.

137   Mice were sacrificed and organs were collected on the 28th day of the administration period.

138

Behavioral experiments

140   Grip strength tests were performed by holding the mice at an automatic grip strength meter

141   (Chatillon DFE II, Columbus Instruments, Columbus, OH, USA) allowing them to grip the grid

142   of the device with their fore- and hindlimbs. Then, mice were gently pulled back by their tail until

143   they released the grip. Force exerted by the mouse during its removal from the grid, as measured

144   by gram force (g), was evaluated 5 times per mouse. For nesting behavior tests, mice were singly

145   caged overnight (16 hours) with a 5 cm x 5 cm cotton nestlet in a clean cage. Produced nests were

146   scored on a scale from 1to 5 as previously described (31). For the tail suspension test, the tails of

the mice were taped to a metal bar attached to the ENV-505TS Load Cell Amplifier and DIG-735

cabinet with high pass filter set to 1 Hz (Med Associates, Fairfax, VT, USA). The time of

immobility was tested over 6 min. For the elevated plus maze test, mice were placed in the center

of a maze consisting of two arms (6 cm x 75 cm), one open and the other enclosed. Over 10 min,

the number of open arm entries was tracked with Ethovision software (Noldus Information

Technology, Leesburg, VA, USA) and normalized to the total amount of arm entries. For the Y

maze test, mice were placed in the center of the Y maze, where the three arms meet and given 8

min to explore. The number of arm alternations is measured relative to total arm entries using

Ethovision software. For the open field test, mice were placed in a 45 cm x 45 cm open top cage

and locomotion was automatically tracked with an overhead-mounted camera connected to a

computer equipped with Ethovision tracking software (Noldus Information Technology). Open

field motor activity was recorded over 10 min. For the hanging wire test, mice were placed on a

wire cage lid which was gently turned upside down over a cage, followed by the recording of the

latency to falling from the lid. Mice were given three consecutive training trials, followed by three

test trials. The average latency to fall was normalized to the body weight of the mouse. Pole tests

were performed by placing the mice on the top of a vertical pole (8 mm diameter and 55 cm height)

with a rough surface. Mice were placed vertically, on the top of the pole, and the time required for

turning was recorded. The mean time to turn was calculated from 5 consecutive trials for each

mouse. For the rotarod test, mice were placed on a rotating, textured rod (IITC Life Science,

Woodland Hills, CA, USA), with the speed gradually increasing from 4 to 40 rpm over 5 min. The

latency to fall from the rotating rod was recorded for every mouse. Four trials per day with 10 min

inter-trial intervals were performed for three consecutive days.

7

170

Tissue harvesting and processing

For biochemical approaches mice were anesthetized with isoflurane (Fresenius Kabi, CP0406V2, Bad Homburg, Germany), and decapitated. Brain tissue of 5-month-old *PAC α-Syn*[A53T] *TG* mice was weighed and lysed 1:3 (w/v) in PEPI buffer (5 mM EDTA, protease inhibitor [GenDEPOT, P3100, Katy, TX, USA] and phosphatase inhibitor [GenDEPOT, P3200] in PBS) with a Dounce homogenizer. Samples were further lysed 1:6 (w/v) using the tissue weight in TSS Buffer (140 mM NaCl, 5 mM Tris–HCl), then TXS Buffer (140 mM NaCl, 5 mM Tris–HCl, 0.5 % Triton X-100), and SDS Buffer (140 mM NaCl, 5 mM Tris–HCl, 1 % SDS), as previously described (32).

For immunohistology with paraffin sections, mice were anesthetized with 120 mg/kg Euthanyl (DIN00141704) and intracardially perfused with 10 mL of PBS, followed by 20 mL of 10 % Buffered Formalin Phosphate (Fisher Scientific, SF100-4). Brains were isolated and fixed in 10 % Buffered Formalin Phosphate at 4 °C for at least 24 hours. After dehydration by 70 %, 80 %, 90 % and 100 % ethanol and clearing by Xylenes, brains were infiltrated and embedded in paraffin (Louise Pelletier Histology Core Facility, University of Ottawa). Brains were sectioned at 5 μm.

SDS-PAGE and mouse protein immunoblots

4X Laemmli buffer (Bio-Rad, 1610747, Hercules, CA, USA) with 20 % 2-mercaptoethanol (Bio-Rad, 1610710) was added to cleared protein and boiled at 95 °C for 5 min. Protein samples were loaded on a 12 % SDS-PAGE gel in the Mini-PROTEAN Tetra Cell (Bio-Rad, 165-8000). Protein was then transferred to a 0.2 μm nitrocellulose membrane (Bio-Rad, 1620112) using the Mini Trans-Blot Electrophoretic Transfer Cell (Bio-Rad, 1703930) in Tris-Glycine buffer with 10 % methanol (Fisher Scientific, A412P) at 340 mA for 90 min at 4 °C. Membranes were then blocked

8

193   in 5 % milk in 1X TBS-T for 1 hour at room temperature followed by overnight incubation in

194   primary antibody against pSer129 (pS) α-Syn (1:2 000, Abcam, 51253, Cambridge, UK), α-Syn

195   (1:2 000, BD Biosciences, 610787, Franklin Lakes, NJ, USA), CDK14 (1:500, Santa Cruz

196   Biotechnology, sc50475, Dallas, Texas, USA) and GAPDH (1:40 000, Proteintech, 60004-1-Ig,

197   Rosemont, IL, USA) diluted in 2 % BSA, 0.02 % NaN_3 in 1X TBS-T. Next, membranes were

198   washed in TBS-T, followed by incubation in secondary antibody (peroxidase-conjugated donkey

199   anti-rabbit IgG, (Cedarlane, 711-035-152, Burlington, ON, Canada) or donkey anti-mouse IgG,

200   (Cedarlane, 715-035-150), both at 1:10 000 diluted in 5 % milk in TBS-T) for 1 hour at RT.

201   Membranes were washed again in TBS-T, bathed in enhanced chemiluminescent reagent (Bio-

202   Rad, 1705061), imaged using the ImageQuant LAS 4100 Imaging system (GE) and quantified

203   using Image Lab 6.1 software (Bio-Rad).

204

205   Dopamine Measurements with liquid chromatography-mass spectrometry/mass

206   spectrometry (LC-MS/MS)

207   Striatal tissue punches from 3 mm thick brain sections from 12-month-old PFF-treated mice were

208   weighed and submitted to The Metabolomics Innovation Centre (TMIC, Edmonton, AB, Canada)

209   for analysis. Samples were homogenized in 50 µL of tissue extraction buffer, followed by

210   centrifugation. Dopamine content in µM was analyzed by reverse-phase LC-MS/MS custom assay

211   in combination with an ABSciex 4000 QTrap® tandem mass spectrometer (Applied Biosystems/

212   MDS Analytical Technologies, Foster City, CA, USA) using isotope-labeled internal standards.

213   The assay utilizes a 96 deep well plate with a filter plate attached on top. Samples were thawed on

214   ice, vortexed and centrifugated at 13 000 x g. 10 µL of sample was loaded in the center of the filter

215   and dried in a stream of nitrogen. Following derivatization by phenyl isothiocyanate and drying of

9

216 filter spots, dopamine content was extracted by adding 300 µL of extraction solvent, centrifugation

217 into the lower collection plate and dilution by MS running solvent. Mass spectrometric analysis

218 was performed with the ABSciex 4000 QTrap® tandem mass spectrometer in combination with

219 an Agilent 1260 series UHPLC system (Agilent Technologies, Palo Alto, CA, USA). Samples

220 were delivered by an LC method followed by a direct injection method. Data was analyzed using

221 Analyst 1.6.2 and expressed as dopamine concentration relative to tissue weight.

222

223 **Histology**

224 For Diaminobenzidine (DAB) antibody staining, paraffin sections were deparaffinized in xylenes

225 and rehydrated in a series of decreasing ethanol (100 %, 90 %, 70 %, 50 %) followed by antigen

226 retrieval in sodium citrate buffer (2.94 g sodium citrate, 0.5 mL Tween 20 in 1 L PBS, pH6) at 80

227 °C for 2 hours and quenching of endogenous peroxidase with 0.9 % H_2O_2 in PBS for 10 min.

228 Sections were blocked in blocking buffer (0.1 % Triton X-100, 10 % normal horse serum in PBS)

229 and incubated in primary antibody (pSer129 α-Syn, 1:500, Abcam, ab51253 or tyrosine

230 hydroxylase, 1:500, Sigma-Aldrich, AB152, St. Louis, MO, USA) overnight at 4 °C. Then,

231 sections were incubated in secondary antibody (donkey anti-rabbit biotin-conjugated, Jackson

232 ImmunoResearch, 711-065-152, West Grove, PA, USA) 1:125 in blocking buffer for 2 hours and

233 tertiary antibody solution (streptavidin-horseradish peroxidase conjugated, 1:250 in blocking

234 buffer, Sigma-Aldrich, RPN1231V) for 2 hours before being exposed to DAB (Vector

235 Laboratories, SK-4100, Newark, CA, USA) for 10 min. Hematoxylin counterstaining was

236 conducted using the hematoxylin and eosin (H&E) Staining Kit (Abcam, ab245880) as per

237 manufacturer's instructions. Stained sections were dehydrated in a series of ethanol and xylenes

238 solutions, followed by mounting sections with Permount (Fisher Scientific, SP15-100) and

239 covering with coverslips.

240 H&E stainings were performed by the Louise Pelletier Histology Core Facility at the University

241 of Ottawa with a Leica Autostainer XL (Leica Biosystems Inc, Concord, ON, Canada). After

242 deparaffinization, sections were exposed to hematoxylin for 7 min and eosin for 30 sec. Then,

243 sections were dehydrated, mounted and covered with coverslips.

244 For immunofluorescence antibody staining, tissue sections and primary neurons were incubated in

245 primary antibody (Synapsin, 1:2 000, Thermo Fisher Scientific, Waltham, MA, USA, A-6442,

246 PSD95, 1:500, Synaptic Systems, Göttingen, Germany, 124 011, pSer129 α-Syn, 1:500, Abcam,

247 ab51253, Map2, 1:5 000, Abcam, ab5392) in blocking buffer overnight at 4 °C. Next,

248 sections/neurons were incubated in secondary antibody (goat anti-rabbit IgG (H+L) Alexa Fluor^{TM}

249 647, Thermo Fisher Scientific, A-21244, for Synapsin, goat anti-mouse IgG (H+L) Alexa Fluor^{TM}

250 488, Thermo Fisher Scientific, A-11001, for PSD95, goat anti-rabbit IgG (H+L) Alexa Fluor^{TM}

251 488, Thermo Fisher Scientific, A-11008, for pS129 α-Syn and goat anti-chicken IgY (H+L) Alexa

252 Fluor^{TM} 647, Thermo Fisher Scientific, A-21449, for Map2, all at 1:500) together with DAPI

253 (Sigma-Aldrich, D9542) for 1 hour at RT, followed by mounting sections with fluorescence

254 mounting medium (Agilent, S302380-2). Brightfield and epifluorescence micrographs were

255 acquired using an Axio Scan Z1 Slide Scanner (Carl Zeiss AG, Oberkochen, Baden-Württemberg,

256 Germany) (20x objective, Louise Pelletier Histology Core Facility) and a Zeiss AxioImager M2

257 (10x objective, Cell Biology and Image Acquisition Core Facility, University of Ottawa) and

258 analyzed using ImageJ (National Institute of Health, Bathesda, MD, USA 1.52p) with 2-3 sections

259 per mouse by a blinded investigator. Heatmaps were generated by counting pS129 α-Syn positive

260 cells in defined regions of the brain (http://atlas.brain-map.org), normalized to the area occupied

11

261 by the region and resulting cell densities were expressed as hues of red. Micrographs of *in situ*

262 hybridization experiments for the expression of *Snca* (experiment 79908848) and *Cdk14*

263 (experiment 71670684) in the mouse brain were downloaded from the Allen Brain Atlas

264 (http://mouse.brain-map.org/) on August 3rd, 2022.

265

266

267 **Cell culture**

268 Cells were kept at 37 °C, 5 % O_2, 10 % CO_2. For primary mouse cortical neurons coverglass #1.5

269 (Electron Microscopy Sciences, Hatfield, PA) were coated for at least 16 hours at 37 °C, washed

270 twice with ddH_2O and air dried at RT. Mouse embryos at embryonic days 14 to 16 were collected

271 from pregnant females from *Cdk14*$^{+/-}$ crossings (anesthetized with 120 mg/kg Euthanyl). Embryos

272 were decapitated, brains removed, cortices isolated in Hank's Balanced Salt Solution (HBSS)

273 (Millipore Sigma, H9394-500ML) and dissociated in 0.7mg/ml trypsin (Sigma-Aldrich, T4549).

274 Cell suspensions were quickly washed with 150 µg/mL trypsin inhibitor (Roche, Basel,

275 Switzerland, 10109878001) and 666.67 µg/mL DNase 1 (Sigma-Aldrich, DN25-10mg), followed

276 by another wash with 10 µg/mL trypsin inhibitor and 83.34 µg/mL DNase 1 and resuspended in

277 neuronal media (Neurobasal Media (Thermo Fisher Scientific, Gibco 21103049), 1X B27

278 supplement (Gibco, 17504044), 1X N2 supplement (Thermo Fisher Scientific, Gibco 17502-048),

279 1X Penicillin Streptomycin (Thermo Fisher Scientific , Gibco SV30010), and 0.5 mM L-glutamine

280 (Wisent Bio Products, Saint-Jean-Baptiste, QC, Canada, 609-065-EL). Single cells were seeded at

281 ~10^5 cells per coverslip and maintained in culture for 9 (**Fig. S1D** and **S2B**) or 21 days (**Fig. 2**).

282 Neurons were treated with 2 µg/mL of sonicated α-Syn PFFs (StressMarq, Victoria, BC, Canada,

283 SPR-324) at 2 (**Fig. S1D** and **S2B**) or 7 days *in vitro* (DIV) (**Fig. 2**). 14 days after adding PFFs to

12

284   the neuronal media, media was extracted and passed through a 40 µm cell strainer (VWR, Radnor,

285   PA, USA, 21008-949) for *in vitro* α-Syn spreading experiments (**Fig. 2**). This conditioned media

286   was added to untreated, naïve wildtype (WT) cortical neuron cultures at the time of the media

287   change (7 DIV) and collected for immunofluorescence experiments at 21 DIV. Neurons treated

288   with conditioned media were analyzed by immunofluorescence quantification after 14 days of

289   treatment at 21 DIV. For immunofluorescence staining, cells were fixed in 4 % PFA for 20 min,

290   washed in PBS and incubated in blocking buffer for 1 hour. Cells were incubated with primary

291   antibodies overnight at 4 ℃, followed by incubation with secondary antibodies for 1 hour at RT.

292

293   **hiPSC culture, neuronal differentiation, and Cas9-mediated gene editing**

294   Human induced pluripotent stem cell (hiPSC) isogenic lines (Female) and human embryonic stem

295   cell (hESC) isogenic lines (Male) were generated as described previously (33). hiPSCs were

296   cultured as previously described (34) with slight modifications. Briefly, pluripotent cells were

297   plated in mTeSR (Stem Cell Technologies, Vancouver, BC, Canada) and media was changed daily.

298   The colonies were manually passaged weekly. Differentiation of hPSCs into A9-type DaNs was

299   performed by following a floor plate differentiation paradigm (34,35). Immediately preceding

300   differentiation, the colonies were dissociated into a single cell suspension using HyQTase. hPSCs

301   were collected and re-plated at 4×10^4 cells/cm^2 on Matrigel (BD Biosciences)-coated tissue culture

302   dishes for differentiation. Floor-plate induction was carried out using hESC-medium containing

303   knockout serum replacement (KSR), LDN193189 (100 nM), SB431542 (10 µM), Sonic Hedgehog

304   (SHH) C25II (100 ng/mL, Purmorphamine (2 µM), Fibroblast growth factor 8 (FGF8; 100 ng/mL),

305   and CHIR99021 (3 µM). On day 5 of differentiation, KSR medium was incrementally shifted to

306   N2 medium (25 %, 50 %, 75 %) every 2 days. On day 11, the medium was changed to

13

307   Neurobasal/B27/Glutamax supplemented with CHIR. On day 13, CHIR was replaced with Brain

308   Derived Neurotrophic Factor (BDNF; 20 ng/mL), ascorbic acid (0.2 mM), Glial Derived

309   Neurotrophic Factor (GDNF; 20 ng/mL), transforming growth factor beta 3 (TGFβ3; 1 ng/mL),

310   dibutyryl cAMP (dbcAMP; 0.5 mM), and DAPT (10 μM) for 9 days. On day 20, cells were

311   dissociated using HyQTase and re-plated under high cell density $4x10^5$ cells/cm^2 in terminal

312   differentiation medium (NB/B27 + BDNF, ascorbic acid, GDNF, dbcAMP, TGFβ3 and DAPT)

313   also referred to as DA Neuron (DAN)-Medium, on dishes pre-coated with poly-ornithine (15

314   μg/mL)/laminin (1 μg/mL)/fibronectin (2 μg/mL). Cells were differentiated for up to 60 DIV, with

315   analysis being performed at DIV14, DIV 45 and/or DIV 60. At D10D and/or D14D of

316   differentiation, hiPSC cultures were transduced with lentivirus containing Cas9 (lentiCRISPR v2,

317   addgene, plasmid #52961) with the following gRNAs: non-targeting (5'-

318   CGCTTCCGCGGCCCGTTCAA-3'), CDK14 exon 3 (5'-GCAAAGAGTCACCTAAAGTT-3')

319   and exon 8 (5'-TGTGCAAAATATAACGCTGG-3'). From D10D-D14D media was

320   supplemented with 0.1 μM compound E (AlfaAesar, J65131, Haverhill, MA, USA). At D18D,

321   cells were replated onto poly-ornithine (15 μg/mL)/laminin (1 μg/mL)/fibronectin (2 μg/mL)

322   coated plates. Cells were maintained in DAN-medium (DMEM/F12, 200uM Ascorbic Acid, 0.5

323   mM dbcAMP, 20 ng/mL BDNF, 20 ng/mL GDNF, 1 ng/mL TGFb3, and 1 % Anti-Anti) for 6-7

324   weeks where lysates were then collected for protein analysis.

325

326   **hESC culture, neuronal differentiation and *in vitro* CDK14 inhibitor treatment**

327   Neural progenitor cell (NPC) differentiation was performed as previously described (36). Dishes

328   for hESC cultures were coated with 0.15 mg/mL growth factor reduced Matrigel (Corning Inc,

329   354230, Corning, NY, USA) in DMEM/F-12 (Thermo Fisher Scientific, 11320033) for 1 hour at

330 RT prior to cell seeding. H9 hESCs (WiCell, WA09, Madison, WI, USA) were seeded as colonies

331 and maintained in mTeSR Plus (StemCell Technologies, 05825). NPC differentiation was initiated

332 when the hESC cultures reached 90 % confluence, by replacing growth medium with Knockout

333 Serum Replacement (KSR) medium (414 mL Knockout-DMEM (Thermo Fisher Scientific,

334 10829018), 75 mL Knockout-serum replacement (Thermo Fisher Scientific, 10828028), 5 mL

335 Glutamax (Thermo Fisher Scientific, 35050061), 5 mL MEM-NEAA (Thermo Fisher Scientific,

336 11140050), 500 µL 2-mercaptoethanol (Thermo Fisher Scientific, 21985023), 500 µL Gentamicin

337 (Wisent Bioproducts 450-135), 10 µM SB431542 (Tocris, 1614, Bristol, UK) and 500 nM LDN-

338 193189 (Stemgent 04-0074, Reprocell Inc, Yokohama, Kanagawa 222-0033, Japan).

339 Differentiation medium was replaced daily on days 4 and 5 by 75:25 KSR:N2 medium (486.5 mL

340 DMEM/F-12 (Thermo Fisher Scientific, 11320033), 5 mL 15 % glucose, 5 mL N2 supplement

341 (Thermo Fisher Scientific, 17502048), 500 µL 20 mg/mL human insulin (Wisent Bioproducts,

342 511-016-CM), 2.5 mL 1M HEPES (Thermo Fisher Scientific, 15630080), 500 µL Gentamicin),

343 on days 6 and 7 by 50:50 KSR:N2, on days 8 and 9 by 25:75 KSR:N2 and on days 10 and 11 by

344 N2 medium containing 500 nM LDN-193189. On day 12, differentiated NPCs were treated with

345 Y-27632 (Tocris, 1254) for 4 hours, dissociated with Accutase (Stemcell Technologies, 07922)

346 and seeded into Matrigel coated dishes containing Neural Induction Medium (NIM, 244 mL

347 DMEM/F12, 244 mL Neurobasal medium (Thermo Fisher Scientific, 21103049), 2.5 mL N2

348 Supplement, 5 mL B-27 Supplement (Thermo Fisher Scientific, 17504044), 2.5 mL GlutaMAX™

349 (Thermo Fisher Scientific, 35050061), 125 µL 20 mg/mL human insulin, 500 µL 20 µg/mL FGF2

350 (StemBeads, SB500, Rensselaer, NY, USA), 10 µL 1 mg/mL hEGF (Millipore Sigma E9644) and

351 500 µL Gentamicin) for expansion. NPCs were passaged at full confluence a minimum of one

352 time before neuronal differentiation.

15

353   For NPC-neuronal differentiation culture dishes were coated with 0.001 % Poly-L-ornithine

354   (Millipore Sigma, P4957) at 4 °C overnight, followed by 25 µg/mL laminin (Millipore Sigma,

355   L2020) for 2 hours at room temperature. NPCs were treated with Y-27632 for 4 hours, dissociated

356   with Accutase and seeded at a density of 20 000 cells/cm^2 in NIM. Neuronal differentiation was

357   initiated when NPCs reached 70 % confluence by replacing growth medium with neuronal

358   differentiation medium (244 mL DMEM/F-12 medium, 244 mL Neurobasal medium, 2.5 mL N2

359   supplement, 5 mL B27 supplement, 200 µL 50 µg/ml BDNF (Peprotech, 450-02), 200 µL 50 µg/ml

360   GDNF (Peprotech 450-10, Thermo Fisher Scientific), 250 mg dibutyryl cyclic-AMP (Millipore

361   Sigma, D0627), 500 µL 100 M L-ascorbic acid (FujiFim Wako Chemicals, 323-44822, Osaka,

362   Japan), and 500 µL Gentamicin). Cells were fed every 3 days for 18 days to obtain immature

363   neuronal networks. FMF-04-159-2 was dissolved in DMSO (Fisher Scientific, BP231) and applied

364   in cell culture medium to hESC-derived neurons for 6 days (with a replenishment of FMF-04-159-

365   2 -containing medium after the first 3 days). For protein analysis cells were washed with cold PBS,

366   scraped, and collected in low protein binding microcentrifuge tubes (Thermo Scientific, 90410).

367   Cells were pelleted by centrifugation at 1 000 x g for 5 min at 4 °C. The supernatant was aspirated,

368   and the cells were lysed in cold RIPA buffer (50 mM Tris, pH 7.5, 150 mM NaCl, 0.1 % SDS, 0.5

369   % sodium deoxycholate; 1 % NP-40, 5 mM EDTA, pH 8.0) with protease and phosphatase

370   inhibitors. Cell lysates were incubated on ice for 20 min, with vortexing every 5 min. Lysates were

371   centrifuged at 18 000 x *g* for 20 min at 4 °C to pellet cell debris.

372

373   **ELISA (Enzyme-Linked ImmunoSorbent Assay)**

374   ELISA α-Syn protein quantification was performed as previously described (37,38). 384-well

375   MaxiSorp plates (Nunc, Inc) were coated with capturing antibody (α-Syn, BD Biosciences,

16

610787) diluted 1:500 in coating buffer (NaHCO$_3$ with 0.2 % NaN3, pH9.6) overnight at 4 °C. Following 3 washes with PBS/0.05 % Tween 20 (PBS-T), plates were blocked for 1 hour at 37 °C in blocking buffer (1.125 % fish skin gelatin; PBS-T). After 3 washes, samples were loaded in duplicates and incubated at RT for 2 hours. Biotinylated hSA4 antibody (in-house antibody) was generated using 200 µg Sulfo-NHS-LC Biotin (Pierce, Thermo Fisher Scientific), diluted 1:200 in blocking buffer and added to the plate for 1 hour at 37 °C. Following 5 washes, ExtrAvidin phosphatase (Sigma, E2636) diluted in blocking buffer was applied for 30 min at 37 °C. Color development was carried out by using fast-p-nitrophenyl phosphate (Sigma, N1891) and monitored at 405 nm every 2.5 min for up to 60 min. Saturation kinetics were examined for identification of time point(s) where standards and sample dilutions were in the log phase.

Primary rat neurons, human α-Syn PFFs and protein analysis

Cortical neurons were harvested from the E18 Sprague Dawley rat embryos (Charles River, Wilmington, MA, USA). The harvested cortical tissue was digested using 17 U/mg Papain followed by mechanical dissociated by gentle trituration through a glass flamed Pasteur pipet. The cells were seeded into plates coated 24 hours prior to dissection with Poly-D-Lysine (0.15 mg/mL). The cells were incubated at 37 °C, 7.5 % CO$_2$ until collection. Every 3 to 4 days, a 50 % media change was performed (2 % B27 supplement, 1 % antibiotic/antimycotic, 0.7 % BSA Fraction V, 0.1 % β-mercaptoethanol in HEPES-buffered DMEM/F12). Where required, cells were exposed to 100 nM FMF-04-159-2 (Bio-Techne, 7158/10, Minneapolis, MN, USA) dissolved in DMSO, at 14 DIV, and again at the subsequent feed (18 DIV). At 14 DIV, cells were exposed to either 1 µg/mL human α-Syn PFFs, or 1 µg/mL monomeric α-Syn. Cell lysates were collected at day 5 post PFF or monomeric exposure. Human α-Syn protein was isolated from BL21-CodonPlus

17

399   (DE3)-RIPL competent cells transformed with pET21a-alpha-synuclein and purified by Reversed-

400   phase HPLC. PFFs were then generated as previously described (39). Purified α-Syn (5 μg/mL in

401   PBS) was incubated at 37 °C with constant shaking for 7 days, then aliquot and stored at -80 °C.

402   Prior to use, PFFs were thawed and diluted in PBS, then subjected to sonication (20% amplitude,

403   30 seconds; 1 second on, 1 second off) and added to neuronal media for exposure to neurons at a

404   concentration of 1 μg/mL for 24 hours. Following the incubation, cell lysates were collected in

405   150 μL ice-cold RIPA buffer containing phosphatase and protease inhibitors (1 mM aprotinin, 1

406   mM sodium orthovanadate, 1 nM sodium fluoride, and 10 mM phenylmethylsulfonyl fluoride).

407   Samples were homogenized using an 18G needle, left on ice to rest for 15 min, and then

408   centrifuged at 14 000 g to remove any cellular debris. For the soluble fraction, cells were lysed in

409   1 % Tx-100 in TBS buffer (TXS buffer) and cleared by ultracentrifugation at 100 000g for 30 min.

410   Pellets were washed twice with 1 % Tx-100 in TBS, then resuspended in 8M Urea + 8 % SDS in

411   TBS buffer (Urea buffer) to generate the insoluble fraction. Using the BioRad DC Protein Assay

412   kit, the protein concentration of each sample was quantified following the manufacturer's

413   guidelines. SDS-PAGE was performed using 12.5 % resolving gels and 4 % stacking gels, and

414   gels were run for 15 min at 80 V followed by approximately 1.5 hours at 110 V. The gels were

415   transferred onto 0.2 μM nitrocellulose membranes at 35 V and 4 °C overnight. Following the

416   transfer, the membranes were blocked for 1 hour at room temperature using blocking buffer (5 %

417   non-fat dry milk in 1 X TBST) with constant agitation. Primary antibodies were prepared in

418   blocking buffer containing 0.1 % Tween 20 and were probed overnight at 4 °C under constant

419   agitation (CDK14, 1:1 000, Santa Cruz Biotechnology, sc50475; TH, 1:1 000, Pel Freeze

420   Biologicals, Rogers, AR, USA, P40101; a-Syn, 1:1 000, BD Biosciences, 610787; pS129 a-Syn,

421   1:500, abcam, ab51253; β-Actin, 1:1 000, rabbit, Biolegend, San Diego, CA, USA, 622101 or

18

422   mouse, Sigma, A5411, βIII-Tubulin, 1:5 000, rabbit, Biolegend, 802001). Following primary

423   antibody incubation, membranes were rinsed using 1XPBS containing 0.1 % Tween 20 and

424   subsequently re-blocked using the blocking buffer. The membranes were then probed with

425   secondary antibody for 1 hour at RT in blocking buffer containing 0.1 % Tween 20 (Goat anti-

426   Mouse IgG (H+L) Secondary Antibody, HRP (Thermo Fisher Scientific, 31430); Goat anti-Rabbit

427   IgG (H+L) Secondary Antibody, HRP (Thermo Fisher Scientific, 31460); Li-Cor infrared

428   conjugated secondary/ IRDye 800RD Donkey anti-Rabbit IgG antibody (LI-COR Biosciences,

429   926-32211, Lincoln, NE, USA) at dilutions of 1:2 000). The membranes were rinsed to remove

430   any residual blocking buffer using 1X PBS containing 0.1 % Tween 20. If HRP-conjugated

431   secondary antibodies were used, membranes were probed for 5 minutes with clarity Western

432   enhanced chemiluminescence blotting substrate (Bio-Rad) and visualized with photosensitive

433   film. For LiCOR-secondary antibodies, membranes were visualized with a LiCOR Odyssey Fc.

434   Total protein was visualized by Coomassie Brilliant Blue (0.1 % Coomassie, 50 % Methanol and

435   10 % glacial acetic acid in ddH$_2$O).

436

Statistics

438   Statistical analysis was performed using GraphPad Prism version 9.2.0. Quantified data are

439   visualized as mean + standard error of the mean (SEM). Unpaired student's *t* tests were used for

440   two-group comparisons. Data affected by one or two factors were analyzed by one-way or two-

441   way analysis of variance (ANOVA), respectively, followed by Bonferroni *post hoc* comparisons

442   (unless otherwise stated in the figure legend) when at least one of the main factors or the interaction

443   was significant. A significance level of 0.05 was accepted for all tests. Asterisks mark *P* values ≤

444   0.05 (*), ≤ 0.01 (**), ≤ 0.001 (***), or ≤ 0.001 (****).

19

RESULTS

CDK14 ablation limits grip strength deficits and reduces cortical α-Syn pathology in PFF-injected mice

We first examined existing *in situ* hybridization data for the expression of *Snca* and *Cdk14* in the murine brain. We observed that both genes are expressed in similar brain regions, including the hippocampus and the SN (**Fig. S1A**). Since PD is a chronic disease, inhibition of a candidate modifier would have to be safe in the long term. We analyzed Cdk14 protein levels in different mouse organs and tested the effects of Cdk14 depletion on survival, fertility, and organ cytoarchitecture *in vivo*. We found that CDK14 protein is highly abundant in the brain, as well as in the lung and the spleen (**Fig. S1B**). Cdk14 nullizygous mice are viable, fertile, and exhibited normal brain morphology (**Fig. S1C**, (27)) and synaptic integrity (**Fig. S1D**). Furthermore, we did not observe altered morphology of the lung and spleen by Cdk14 ablation (**Fig. S1E**). We next asked whether silencing *Cdk14* is sufficient to mitigate behavioral and histological phenotypes observed in cultured neurons and in mice exposed to pathogenic α-Syn pre-formed fibrils (mouse PFFs; **Fig. 1A** and **B**; **Fig. S2A**). 6 months following intrastriatal injection of α-Syn PFFs, there is a stereotypic brain-wide accumulation of pS129 α-Syn – a marker of human synucleinopathies – in addition to SN DaNs loss and mild motor impairments (40–42). In our experimental paradigm, 6 months after PFF injection (at an age of 12 months), we found that PFF injected WT mice exhibited reduced forelimb force generation in the grip strength test compared to their saline-treated counterparts (**Fig. 1B**), similar to what has been previously reported (41,42). In contrast, the PFF-induced weakening of grip strength was not observed in *Cdk14*$^{+/-}$ or in *Cdk14*$^{-/-}$ mice. We did not observe PFF-mediated changes (in any genotype tested) in the other 8 behavioral tests

468   conducted (including tests for cognitive and motor function). Importantly, we noted that saline-

469   injected *Cdk14*$^{+/-}$ and *Cdk14*$^{-/-}$ mice consistently performed like their WT counterparts in each test,

470   suggesting that chronic Cdk14 reduction is not deleterious to the brain (**Fig. S2C**).

471   Next, we analyzed the relative pathological burden of accumulated α-Syn throughout the brain of

472   mice injected with PFFs. We stained for synucleinopathy-linked pS129

473   α-Syn in the brain of WT mice and found high amounts of pS129 α-Syn-positive cells in the PFF-

474   injected hemisphere (ipsilateral to the injection, IL), which were absent in saline-injected controls

475   (data not shown). We then mapped the distribution of α-Syn pathology at three different

476   rostrocaudal levels near the injection site (relative to bregma: +0.98 mm, +0.26 mm and -1.34 mm)

477   and found an overall blunting of pS129 α-Syn-positive pathology in the PFF-injected *Cdk14*$^{+/-}$ and

478   *Cdk14*$^{-/-}$ mice compared to their WT littermates (**Fig. 1C**). This was particularly evident at

479   anatomical regions distal from the injection site, such as the somatomotor cortex (bregma +0.26

480   mm) and in other cortical areas. Surprisingly, α-Syn pathology proximal to the injection site in the

481   striatum was not significantly affected between PFF-injected genotypes (**Fig. 1C**). Similarly to

482   cortical regions of PFF-injected *Cdk14*$^{-/-}$ mice, we observed fewer pS129 α-Syn-positive neurons

483   in *Cdk14*$^{-/-}$ mouse primary cortical cultures treated with PFFs compared to their WT littermate

484   controls (**Fig. S2B**).

485   Previous reports have shown that α-Syn PFFs can induce nigrostriatal degeneration over time

486   (40–42). We stained for tyrosine hydroxylase (TH) at the injection site in the striatum and observed

487   a similar decrease of TH-positive dopamine fibers in WT, *Cdk14*$^{+/-}$ and *Cdk14*$^{-/-}$ mice injected with

488   PFFs ipsilateral to the injection, relative to their saline-treated counterparts (**Fig. 1D**). PFF-induced

489   loss of dopamine fibers was not accompanied by altered striatal dopamine content (**Fig. S2D**). TH

490   staining in the midbrain revealed equal loss of SN DaNs in PFF-injected WT, *Cdk14*$^{+/-}$ and

491 *Cdk14^{-/-}* mice in comparison to saline-injected controls (**Fig. S2D**). Together, these data show that

492 loss of Cdk14 blunts cortical α-Syn histopathology and PFF-induced grip strength impairment

493 without evidently halting nigrostriatal neurodegeneration in the PFF model. It was interesting to

494 note that the effect of Cdk14 on α-Syn was selective to pathological forms of the protein, as partial

495 reduction or ablation of Cdk14 in *Cdk14^{+/-}* or *Cdk14^{-/-}* mice, respectively, did not change levels of

496 endogenous mouse α-Syn (**Fig. S2E**).

497

498 **Cdk14 loss decreases α-Syn cell-to-cell spread in cortical neuron culture**

499 Our *in vivo* data suggest that decreasing Cdk14 reduces distal (e.g. contralateral; higher cortical

500 area) pathology, while not affecting pathology close to the injection site. We hypothesized that

501 Cdk14 may preferentially affect the cell-to-cell spread of α-Syn, thus contributing to this

502 phenomenon. To test this, we cultured primary neurons of WT, *Cdk14^{+/-}* and

503 *Cdk14^{-/-}* embryos, treated them with mouse PFFs at 7 days in culture and collected media 14 days

504 post PFF application (a time where most of the exogenous fibrils have been depleted from the

505 system ((43); schematic in **Fig. 2A**). We applied this filtered, seed-competent media to naïve WT

506 cultures to test the seeding capacity of α-Syn and found that loss of Cdk14 dramatically reduced

507 α-Syn pathology (measured by pS129 α-Syn accumulation), 14 days following media application

508 (**Fig. 2B**).

509

510 **Knockdown of CDK14 decreases pS129 α-Syn levels in human neurons**

511 Having observed the benefits of Cdk14 depletion in the PFF mouse model of PD, we next tested

512 whether this benefit translates to human neurons. We infected DaNs derived from a PD patient

513 carrying an A53T mutation in α-Syn (33) as well as its isogenic control with lentiviruses carrying

22

514   Cas9/sgRNAs against *CDK14*. Neurons infected with sgRNAs targeting either exon 3 (E3) or exon

515   8 (E8) of *CDK14*, exhibited approximately 50 % of the CDK14 levels of the control cultures (**Fig.**

516   **3**). We found that A53T mutant cells show a marked increase of pS129 α-Syn compared to isogenic

517   controls, and that *CDK14* knockdown significantly lowers pS129 α-Syn levels (**Fig. 3**).

518

519   **Pharmacological targeting of CDK14 decreases α-Syn levels and mitigates its pathogenic**

520   **accumulation**

521   As kinases are typically druggable targets which can be inhibited in non-invasive ways (44), we

522   next asked whether CDK14 inhibition would be a tractable route for decreasing α-Syn levels. We

523   used a recently developed CDK14 covalent inhibitor (FMF-04-159-2) (26) to test whether acute

524   inhibition of CDK14 reduces α-Syn levels. We treated hESC-derived cortical neurons with the

525   CDK14 inhibitor for 6 days and observed a dose-dependent reduction in total α-Syn concentration

526   by ELISA (**Fig. 4A**). We also tested whether the CDK14 inhibitor affects the α-Syn load in rat

527   primary neuronal cultures treated with α-Syn PFFs. Here, PFF treatment induced a spike in

528   insoluble (Urea buffer-soluble) α-Syn protein, which CDK14 inhibition markedly reduced (**Fig.**

529   **4B**). Interestingly, the PFF treatment also induced an increase of CDK14 insoluble protein, which

530   was not present in untreated neurons or in neurons treated with α-Syn monomers (**Fig. 4B**).

531

532   ***In vivo*** **inhibition of CDK14 decreases the load of human α-Syn**

533   Since the treatment of human neurons and PFF-challenged rat neurons with the CDK14 inhibitor

534   showed a reduction in total and insoluble α-Syn protein, respectively, we next tested whether

535   pharmacological inhibition of CDK14 modifies α-Syn levels *in vivo*. We administered FMF-04-

536   159-2 via intracerebroventricular infusion at 0.35 mg/kg/day for 28 days in 4-month-old *PAC α-*

23

537 *Syn*^A53T *TG* mice (**Fig. 5A**) which harbor the PD-associated A53T mutant human α-Syn gene in

538 the absence of mouse *Snca* (28). Administration of the CDK14 inhibitor did not modify body

539 weight development, nor induce any signs of distress or pain as indicated by alterations of

540 locomotion, facial expression, or coat condition of *PAC α-Syn*^A53T *TG* mice in comparison to

541 vehicle-treated counterparts (**Fig. S3A**). Similarly, CDK14 inhibitor treatment did not induce

542 changes in the cytoarchitecture of the lung, spleen, and liver (**Fig. S3B**). To quantify levels of

543 pathogenic forms α-Syn, we collected brains after 1 month of CDK14 inhibitor treatment (**Fig.**

544 **5A**) and analyzed protein content of the TSS, TXS and SDS buffer-soluble fractions (**Fig. 5B**). We

545 observed a reduction of total α-Syn and low molecular weight α-Syn species, suggestive of

546 decreased C-terminally truncated (CTT) α-Syn in CDK14 inhibitor-treated mice relative to their

547 vehicle controls. Interestingly, levels of pS129 α-Syn were increased in CDK14 inhibitor treated

548 mice in the TSS buffer-soluble fraction, whereas it was decreased in the TXS buffer-soluble

549 fraction. Notably, CDK14 levels were specifically decreased (target engagement) in the TXS and

550 SDS buffer-soluble fractions, but not the TSS buffer-soluble fraction, of inhibitor-treated mice.

551 Together these results show that *in vivo* administration of the CDK14 inhibitor in the brain engages

552 its target and mitigates certain pathogenic forms of human α-Syn in the mouse brain in a protein

553 fraction-dependent manner without inducing obvious discomfort or pain.

554

555 **DISCUSSION**

556 α-Syn is increasingly considered a valid experimental therapeutic target for PD, based on clinical

557 genetic and neuropathological evidence, as well as animal and cell culture studies. *SNCA* gene

558 mutations or amplifications resulting in α-Syn pathology are tightly linked to PD pathogenesis.

559 Moreover, α-Syn is a major constituent of Lewy-like structures, the pathological hallmark of PD

24

560   and related synucleinopathies. Thus, targeting α-Syn has been a major thrust in the pharmaceutical

561   realm. One aspect of α-Syn pathology that has been difficult to overcome is the notion that different

562   states of its post-translational modification or aggregation differentially affect disease

563   pathogenesis: a clear image has yet to emerge as to the real culprit of α-Syn toxicity. Although

564   novel strategies such as anti-sense oligonucleotides, immunotherapy and small molecule inhibitors

565   of α-Syn aggregation are being explored (45), finding a target that can be pharmacologically

566   inhibited still holds potential as a minimally invasive and simple strategy to lower α-Syn levels –

567   especially when such treatment course would be made over several decades. Indeed, a growing

568   body of evidence suggests that α-Syn may play a role not only at the presynaptic space but also in

569   the immune system (37,46,47). Therefore, careful titration of its levels may be clinically crucial.

570   As a result, we asked whether candidates that are more amenable to traditional pharmacology (i.e.

571   kinases) could regulate α-Syn dosage, irrespective of its aggregation status. Our previous studies

572   identified a handful of these modifiers including TRIM28 and DCLK1 (8,22,48,49). Here, we

573   study a heretofore unexplored target as well as its newly developed cognate inhibitor (26) for

574   disease modification in pre-clinical models of PD: CDK14.

575   We show that the reduction of CDK14 protein levels is well tolerated and causes a reduction

576   in pathogenic α-Syn accumulation in murine and human models of synucleinopathy. Genetic

577   suppression of *Cdk14* reduces pS129 α-Syn pathology in the cortex of PFF-injected mice and

578   dampens the development of grip strength deficits in these mice; while this rescue is not found at

579   sites proximal to the injection, including the nigrostriatal tract. Importantly, the genetic reduction

580   of CDK14 in DaNs derived from an individual with synucleinopathy shows equal promise in

581   preventing phenotypic development. We show that the selective covalent CDK14 inhibitor, FMF-

582   04-159-2, decreases α-Syn levels in hESC-derived human neurons and mitigates PFF-induced α-

25

583 Syn pathology in rat cortical neurons. Lastly, we demonstrate that administering FMF-04-159-2

584 *in vivo* reduces α-Syn dosage and, consequently, decreases pathogenic forms of α-Syn in a

585 humanized mouse line expressing PD-linked A53T *SNCA*. Collectively, these results show that

586 CDK14 is a pharmacologically tractable target for synucleinopathy.

587 　　We observed that loss of Cdk14 in PFF-treated mice reduced the level of α-Syn

588 histopathology in cortical areas, such as the somatomotor cortex. Surprisingly, we did not detect

589 changes in the load of pS129 α-Syn-positive cells by *Cdk14* ablation in the striatum, the PFF

590 injection site (**Fig. 1C**). In line with this, we noticed a similar PFF-induced degeneration of the

591 dopaminergic nigrostriatal system in WT, *Cdk14$^{+/-}$* and *Cdk14$^{-/-}$* mice (**Fig. 1D** and **Fig. S2D**).

592 These observations imply that loss of CDK14 reduces the degree of intercellular α-Syn spreading

593 rather than protecting neurons which are directly exposed to PFFs. Indeed, when we tested this in

594 a cultured neuron system, we found that genetic reduction of Cdk14 dramatically decreased the

595 spreading capacity of seed-competent α-Syn (**Fig. 2**). Therefore, it is plausible that CDK14

596 facilitates the cell-to-cell spread of α-Syn. Genetic reduction of CDK14 using a CRISPR/Cas9-

597 mediated strategy in stem cell-derived human neurons carrying the PD-linked *SNCA* A53T

598 mutation lowered levels of pS129 α-Syn (**Fig. 3**), indicating that ablation of both, murine and

599 human *Cdk14*/*CDK14* mitigates the neuronal load of this pathology-linked form of α-Syn.

600 　　Given the lack of phenotypes in the *Cdk14$^{-/-}$* or *Cdk14$^{+/-}$* mice, no evidence for loss of

601 function intolerance in humans (probability of loss of function intolerance [pLI] = 0; gnomAD

602 database, *CDK14* | gnomAD v2.1.1), (50)) and the availability of a recently developed highly

603 selective CDK14 inhibitor, we further explored the pharmacological tractability of CDK14 in the

604 context of synucleinopathy. Treatment of hESC-derived cortical neurons with the newly developed

605 CDK14 inhibitor FMF-04-159-2 induced a pronounced reduction of the total α-Syn concentration,

26

606   as measured by ELISA quantification (**Fig. 4A)**. FMF-04-159-2 was recently designed to provide

607   an improved pharmacological tool for the inhibition of CDK14 as treatment for colorectal cancer

608   (26). Interestingly, FMF-04-159-2 was described to covalently bind and inhibit CDK14 at ~100

609   nM ($IC_{50} = 86$ nM (26)), a dosage which lowered α-Syn levels to ~12 % of vehicle-treated controls

610   in our *in vitro* experiments. Applying the CDK14 inhibitor to PFF-challenged rat cortical neurons

611   reduced the amount of aggregated (Urea buffer-soluble) α-Syn species (**Fig. 4B**), phenocopying

612   the low degree of pS129 pathology in cortical neurons of PFF-treated *Cdk14*^{-/-} mice (**Fig. 1C**) or

613   cultures (**Fig. 2** and **Fig. S2B**). Interestingly, we found that Cdk14 accumulated in the urea-soluble

614   fraction, specifically upon PFF treatment. To our knowledge, it is not known whether CDK14 is

615   present in LBs or LNs in brains of PD patients. Future histopathology experiments may generate

616   deeper insights on if CDK14 aggregates together with α-Syn in patients with synucleinopathies.

617   Comparable to CDK14 inhibitor-treated rat neurons with PFFs, we observed a reduction of total

618   α-Syn in the more insoluble, TXS buffer-soluble protein fraction (and in the TSS buffer-soluble

619   fraction) of *PAC α-Syn*[A53T] *TG* mice which received FMF-04-159-2 via intracerebral injection

620   (**Fig. 5A** and **B**). Reduction of total α-Syn was accompanied by lower amounts of CTT α-Syn,

621   indicating that this form of α-Syn, which increases α-Syn's propensity to aggregate and enhances

622   its cytotoxic effects (51–53), is modulated by CDK14. Levels of pS129 α-Syn were reduced in the

623   more insoluble TXS fraction of CDK14 inhibitor-treated mice, again pointing towards lower

624   degrees of aggregated, pathology-relevant forms of α-Syn. In contrast to these findings, we found

625   paradoxically increased amounts of pS129 α-Syn in the TSS buffer-soluble fraction (highly

626   soluble) of CDK14 inhibitor-treated mice, suggesting that Cdk14 blockage increased pS129 α-Syn

627   in the cytosol of this α-Syn-humanized mouse line. Notably, we did not observe any macroscopic

628   signs of PD/neuropathy-linked behavioral abnormalities in *PAC α-Syn*[A53T] *TG* mice upon CDK14

27

629   inhibitor treatment, such as loss of motor activity or imbalance during locomotion (**Fig. S3A**),

630   implying that higher amounts of cytosolic pS129 α-Syn do not substantially promote cerebral and

631   functional impairments. Elevated levels of cytosolic, non-aggregated pS129 α-Syn seem to be

632   indicative of earlier stages of synucleinopathies, as cytoplasmic networks positive for pS129 α-

633   Syn are more commonly observed in neurons without LBs from patients with early-stage disease,

634   than in LB-containing neurons of patients with advanced PD (54). Based on these *in vivo* CDK14

635   inhibitor administration experiments, we hypothesize that blockage of CDK14 activity reduces

636   loads of pathology-linked forms of insoluble α-Syn, potentially shifting synucleinopathy

637   progression to an earlier phase of disease development.

638   Our experiments provide insights in the modulatory effects on α-Syn pathology by reduced

639   CDK14 activity in neurons from multiple mammalian species. However, we did not observe any

640   direct interaction between both proteins, CDK14 and α-Syn. Moreover, we could not detect any

641   kinase activity of recombinant CDK14 toward wild-type α-Syn *in vitro* (data not shown). We

642   therefore hypothesize that loss or inhibition of CDK14 causes a decrease in α-Syn through

643   unknown mediators, ultimately regulating α-Syn protein levels and intercellular spreading of α-

644   Syn pathology. Future studies will help refine the mechanism whereby CDK14 regulates α-Syn.

645   Our results examining the genetic and pharmacological reduction of CDK14 in PD models

646   set the stage for future pre-clinical studies. In all behavioral experiments conducted, *Cdk14^{-/-}* mice

647   were indistinguishable from WT mice (**Fig. 1B** and **Fig. S2C**). Furthermore, loss of Cdk14 did not

648   alter the architecture of brain tissue or peripheral organs (**Fig. S1C** to **Fig. S1E**) implying that

649   *Cdk14* loss is not deleterious *in vivo*. This is supported by human genetics where the loss of *CDK14*

650   appears to be well tolerated. Additionally, Cdk14 inhibition *in vivo* did not induce any signs of

651   discomfort (**Fig. S3A**), implying that pharmacological targeting of CDK14 is safe. Similarly,

652 systemic administration of FMF-04-159-2 at a ~140-fold higher delivery rate (50 mg/kg/day)

653 appears to be well tolerated by mice as shown in a recent study (55) where Cdk14 inhibition

654 mitigated the growth of lung tumors. In our study, the activity of the CDK14 inhibitor in human

655 neurons appears to be high, affecting CDK14 (and thus α-Syn metabolism) in the nanomolar range

656 (**Fig 4A**). Further preclinical experiments will test whether the drug rescues PD-like neuron loss

657 and behavioral phenotypes in models of synucleinopathies; potentially paving the way for its use

658 in humans.

659   In sum, we show that CDK14 inhibition causes a decrease of total α-Syn concentrations

660 under both *ex vivo* and *in vivo* conditions, ameliorates the levels of pathology-relevant forms of α-

661 Syn and potentially reduces cell-to-cell transmission of α-Syn. Given the strong evidence linking

662 α-Syn levels to PD pathogenesis, we conclude that targeting CDK14 function holds promise as a

663 potentially disease-modifying approach to treat PD.

664

665 **CONCLUSIONS**

666 Elevated α-Syn levels are closely linked to PD. In this study, we explore the effect of inhibiting

667 CDK14 as a pharmacologically tractable approach to decrease α-Syn levels in cultured neurons

668 and animal models. We show that the genetic reduction of Cdk14 mitigates grip strength

669 impairment and ameliorates cortical α-Syn pathology in PFF-treated mice, without affecting

670 nigrostriatal pathology proximal to the injection site; Cdk14 likely acts to regulate the intercellular

671 spread of seed-competent α-Syn. Similarly, *CDK14* ablation reduces α-Syn pathology in human

672 dopaminergic neurons derived from PD patients. Finally, pharmacological targeting of CDK14

673 lowers pathological α-Syn in cultured neurons and modifies pathogenic forms of α-Syn in mice

29

674   expressing PD-linked human A53T *SNCA*. Taken together, we propose CDK14 inhibition as a

675   novel pre-clinical strategy to treat synucleinopathy.

676

677   **LIST OF ABBREVIATIONS**

678   α-Syn: α-Synuclein; BDW: bodyweight; CDK14: cyclin-dependent kinase 14; CL: contralateral;

679   CTT: C-terminally truncated α-Syn; DAB: diaminobenzidine; DaNs: dopaminergic neurons; DIV:

680   days *in vitro*; ELISA: enzyme-linked immunosorbent essay; H&E: hematoxylin and eosin; hESC:

681   human embryonic stem cell; high exp.: high exposure; hiPSC: human induced pluripotent stem

682   cell; IL: ipsilateral; min: minutes; KO: knockout; LC-MS/MS: liquid chromatography – mass

683   spectrometry/mass spectrometry; Mono: α-Synuclein monomers; NPC: neural precursor cell; PBS:

684   phosphate-buffered saline; PD: Parkinson's disease; PFFs: α-Synuclein preformed fibrils; RT:

685   room temperature; sec: seconds; SEM: standard error of the mean; SN: *substantia nigra pars*

686   *compacta*; TG: transgene; UT: untreated; WT: Wildtype

687

688   **DECLARATIONS**

689

690   **Ethics approval and consent to participate**

691   Animal experiments were done under the approved breeding and behavior protocols approved by

692   the University of Ottawa Animal Care Committee. Studies with hESCs were performed following

693   approval by the Stem Cell Oversight Committee of Canada and the Institutional Review Board

694   (Ottawa Health Science Network Research Ethics Board).

695

696   **Consent for publication**

697   Not applicable

698

699   **Availability of data and material**

700   All data of this study are in the main text or in the Supplementary Materials.

701   Cdk14$^{-/-}$ mice were obtained from David S. Park from the University of Calgary and are on an F14

702   C57BL/6N background. *PAC α-Syn*^{A53T} *TG* mice (dbl-PAC-Tg(*SNCA*^{A53T})$^{+/+}$;*Snca*$^{-/-}$, (28)) were

703   provided by Robert L. Nussbaum from the University of California, San Francisco. Any other

704   materials are commercially available.

705

706   **Competing interests**

707   The authors declare that they have no competing interests.

708

727   **Authors' contributions**

31

References and Notes

750 1.   Selvaraj S, Piramanayagam S. Impact of gene mutation in the development of Parkinson's
751   disease. Genes Dis. 2019;6(2):120–8.
752 2.   Mhyre TR, Boyd JT, Hamill RW, Maguire-Zeiss KA. Parkinson's disease. Subcell
753   Biochem. 2012;65:389–455.
754 3.   Sveinbjornsdottir S. The clinical symptoms of Parkinson's disease. J Neurochem.
755   2016;139:318–24.
756 4.   Mazzoni P, Shabbott B, Cortés JC. Motor control abnormalities in Parkinson's disease.
757   Cold Spring Harb Perspect Med. 2012;2(6):1–17.

32

758 5.   Berardelli A, Rothwell JC, Thompson PD, Hallett M. Pathophysiology of bradykinesia in
759   Parkinson's disease. Brain. 2001 Nov;124(11):2131–46.
760 6.   Mor DE, Ischiropoulos H. The Convergence of Dopamine and α-Synuclein: Implications
761   for Parkinson's Disease. J Exp Neurosci. 2018 Mar;12:1179069518761360.
762 7.   Fujiwara H, Hasegawa M, Dohmae N, Kawashima A, Masliah E, Goldberg MS, et al. α-
763   Synuclein is phosphorylated in synucleinopathy lesions. Nat Cell Biol. 2002;4(2):160–4.
764   Available from: https://doi.org/10.1038/ncb748
765 8.   Vázquez-Vélez GE, Gonzales KA, Revelli J-P, Adamski CJ, Alavi Naini F, Bajić A, et al.
766   Doublecortin-like Kinase 1 Regulates α-Synuclein Levels and Toxicity. J Neurosci.
767   2020;40(2):459. Available from: http://www.jneurosci.org/content/40/2/459.abstract
768 9.   Rousseaux MWC, Shulman JM, Jankovic J. Progress toward an integrated understanding
769   of Parkinson's disease [version 1; peer review: 2 approved]. F1000Research.
770   2017;6(1121). Available from: http://openr.es/9uu
771 10. Campêlo CL das C, Silva RH. Genetic Variants in SNCA and the Risk of Sporadic
772   Parkinson's Disease and Clinical Outcomes: A Review. Parkinsons Dis. 2017/07/11.
773   2017;2017:4318416. Available from: https://pubmed.ncbi.nlm.nih.gov/28781905
774 11. Singleton AB, Farrer M, Johnson J, Singleton A, Hague S, Kachergus J, et al. α-Synuclein
775   Locus Triplication Causes Parkinson's Disease. Science (80-). 2003;302(5646):841.
776   Available from: http://science.sciencemag.org/content/302/5646/841.abstract
777 12. Gründemann J, Schlaudraff F, Haeckel O, Liss B. Elevated α-synuclein mRNA levels in
778   individual UV-laser-microdissected dopaminergic substantia nigra neurons in idiopathic
779   Parkinson's disease . Nucleic Acids Res. 2008 Mar 10;36(7):e38–e38. Available from:
780   https://doi.org/10.1093/nar/gkn084
781 13. Feany MB, Bender WW. A Drosophila model of Parkinson's disease. Nature.
782   2000;404(6776):394–8. Available from: https://doi.org/10.1038/35006074
783 14. Masliah E, Rockenstein E, Veinbergs I, Mallory M, Hashimoto M, Takeda A, et al.
784   Dopaminergic Loss and Inclusion Body Formation in α-Synuclein Mice: Implications for
785   Neurodegenerative Disorders. Science (80-). 2000;287(5456):1265. Available from:
786   http://science.sciencemag.org/content/287/5456/1265.abstract
787 15. Lakso M, Vartiainen S, Moilanen A-M, Sirviö J, Thomas JH, Nass R, et al. Dopaminergic
788   neuronal loss and motor deficits in Caenorhabditis elegans overexpressing human α-
789   synuclein. J Neurochem. 2003 Jul 1;86(1):165–72. Available from:
790   https://doi.org/10.1046/j.1471-4159.2003.01809.x
791 16. Chu Y, Kordower JH. Age-associated increases of α-synuclein in monkeys and humans
792   are associated with nigrostriatal dopamine depletion: Is this the target for Parkinson's
793   disease? Neurobiol Dis. 2007;25(1):134–49. Available from:
794   http://www.sciencedirect.com/science/article/pii/S0969996106002191
795 17. Polymeropoulos MH, Lavedan C, Leroy E, Ide SE, Dehejia A, Dutra A, et al. Mutation in
796   the alpha-synuclein gene identified in families with Parkinson's disease. Science. 1997
797   Jun;276(5321):2045–7.
798 18. Stefanis L. α-Synuclein in Parkinson's Disease. Cold Spring Harb Perspect Med . 2012
799   Feb 1;2(2). Available from:
800   http://perspectivesinmedicine.cshlp.org/content/2/2/a009399.abstract
801 19. Sulzer D, Edwards RH. The physiological role of α-synuclein and its relationship to
802   Parkinson's Disease. J Neurochem. 2019 Sep 1;150(5):475–86. Available from:
803   https://doi.org/10.1111/jnc.14810

33

804   20.   Becket G-H, Manuela P, Megumi M-T, Ling D, M. WA, H. NE, et al. αβγ-Synuclein
805   triple knockout mice reveal age-dependent neuronal dysfunction. Proc Natl Acad Sci.
806   2010 Nov 9;107(45):19573–8. Available from: https://doi.org/10.1073/pnas.1005005107
807   21.   Kokhan VS, Afanasyeva MA, Van'kin GI. α-Synuclein knockout mice have cognitive
808   impairments. Behav Brain Res. 2012;231(1):226–30.
809   22.   Rousseaux MWC, Vázquez-Vélez GE, Al-Ramahi I, Jeong H-H, Bajić A, Revelli J-P, et
810   al. A Druggable Genome Screen Identifies Modifiers of α-Synuclein Levels via a Tiered
811   Cross-Species Validation Approach. J Neurosci. 2018;38(43):9286. Available from:
812   http://www.jneurosci.org/content/38/43/9286.abstract
813   23.   Shu F, Lv S, Qin Y, Ma X, Wang X, Peng X, et al. Functional characterization of human
814   PFTK1 as a cyclin-dependent kinase. Proc Natl Acad Sci U S A. 2007/05/21. 2007 May
815   29;104(22):9248–53. Available from: https://pubmed.ncbi.nlm.nih.gov/17517622
816   24.   Chen L, Wang Y, Jiang W, Ni R, Wang Y, Ni S. CDK14 involvement in proliferation
817   migration and invasion of esophageal cancer. Ann Transl Med. 2019 Nov;7(22):681.
818   Available from: https://pubmed.ncbi.nlm.nih.gov/31930082
819   25.   Zhou Y, Rideout WM, Bressel A, Yalavarthi S, Zi T, Potz D, et al. Spontaneous genomic
820   alterations in a chimeric model of colorectal cancer enable metastasis and guide effective
821   combinatorial therapy. PLoS One. 2014;9(8):1–13.
822   26.   Ferguson FM, Doctor ZM, Ficarro SB, Browne CM, Marto JA, Johnson JL, et al.
823   Discovery of Covalent CDK14 Inhibitors with Pan-TAIRE Family Specificity. Cell Chem
824   Biol. 2019;26(6):804-817.e12. Available from:
825   http://www.sciencedirect.com/science/article/pii/S2451945619300704
826   27.   Rodríguez González Y, Kamkar F, Jafar-nejad P, Wang S, Qu D, Sanchez Alvarez L, et
827   al. PFTK1 kinase regulates axogenesis during development via RhoA activation. bioRxiv.
828   2022 Jan 1;2022.01.11.475789. Available from:
829   http://biorxiv.org/content/early/2022/03/10/2022.01.11.475789.abstract
830   28.   Kuo Y-M, Li Z, Jiao Y, Gaborit N, Pani AK, Orrison BM, et al. Extensive enteric nervous
831   system abnormalities in mice transgenic for artificial chromosomes containing Parkinson
832   disease-associated alpha-synuclein gene mutations precede central nervous system
833   changes. Hum Mol Genet. 2010/01/27. 2010 May 1;19(9):1633–50. Available from:
834   https://pubmed.ncbi.nlm.nih.gov/20106867
835   29.   Volpicelli-Daley LA, Luk KC, Patel TP, Tanik SA, Riddle DM, Stieber A, et al.
836   Exogenous α-synuclein fibrils induce Lewy body pathology leading to synaptic
837   dysfunction and neuron death. Neuron. 2011 Oct 6;72(1):57–71. Available from:
838   https://pubmed.ncbi.nlm.nih.gov/21982369
839   30.   Polinski NK, Volpicelli-Daley LA, Sortwell CE, Luk KC, Cremades N, Gottler LM, et al.
840   Best Practices for Generating and Using Alpha-Synuclein Pre-Formed Fibrils to Model
841   Parkinson's Disease in Rodents. J Parkinsons Dis. 2018;8(2):303–22. Available from:
842   https://pubmed.ncbi.nlm.nih.gov/29400668
843   31.   Deacon R. Assessing burrowing, nest construction, and hoarding in mice. J Vis Exp. 2012
844   Jan 5;(59):e2607–e2607. Available from: https://pubmed.ncbi.nlm.nih.gov/22258546
845   32.   Geertsma HM, Suk TR, Ricke KM, Horsthuis K, Parmasad J-LA, Fisk ZA, et al.
846   Constitutive nuclear accumulation of endogenous alpha-synuclein in mice causes motor
847   impairment and cortical dysfunction, independent of protein aggregation. Hum Mol
848   Genet. 2022 Feb 18;ddac035. Available from: https://doi.org/10.1093/hmg/ddac035
849   33.   Soldner F, Laganière J, Cheng AW, Hockemeyer D, Gao Q, Alagappan R, et al.

Generation of Isogenic Pluripotent Stem Cells Differing Exclusively at Two Early Onset Parkinson Point Mutations. Cell. 2011;146(2):318–31. Available from: https://www.sciencedirect.com/science/article/pii/S0092867411006611

34. Ryan SD, Dolatabadi N, Chan SF, Zhang X, Akhtar MW, Parker J, et al. Isogenic Human iPSC Parkinson's Model Shows Nitrosative Stress-Induced Dysfunction in MEF2-PGC1α Transcription. Cell. 2013;155(6):1351–64. Available from: http://www.sciencedirect.com/science/article/pii/S0092867413014220

35. Kriks S, Shim J-W, Piao J, Ganat YM, Wakeman DR, Xie Z, et al. Dopamine neurons derived from human ES cells efficiently engraft in animal models of Parkinson's disease. Nature. 2011;480(7378):547–51. Available from: https://doi.org/10.1038/nature10648

36. Delaney SP, Julian LM, Pietrobon A, Yockell-Lelièvre J, Doré C, Wang TT, et al. Human pluripotent stem cell modeling of tuberous sclerosis complex reveals lineage-specific therapeutic vulnerabilities. bioRxiv. 2020 Jan 1;683359. Available from: http://biorxiv.org/content/early/2020/02/14/683359.abstract

37. Tomlinson JJ, Shutinoski B, Dong L, Meng F, Elleithy D, Lengacher NA, et al. Holocranohistochemistry enables the visualization of α-synuclein expression in the murine olfactory system and discovery of its systemic anti-microbial effects. J Neural Transm. 2017;124(6):721–38. Available from: https://doi.org/10.1007/s00702-017-1726-7

38. Bojan S, Mansoureh H, E. HI, Michaela L, Juliana R, Nathalie L, et al. Lrrk2 alleles modulate inflammation during microbial infection of mice in a sex-dependent manner. Sci Transl Med. 2019 Sep 25;11(511):eaas9292. Available from: https://doi.org/10.1126/scitranslmed.aas9292

39. Volpicelli-Daley LA, Luk KC, Lee VM-Y. Addition of exogenous α-synuclein preformed fibrils to primary neuronal cultures to seed recruitment of endogenous α-synuclein to Lewy body and Lewy neurite–like aggregates. Nat Protoc. 2014;9(9):2135–46. Available from: https://doi.org/10.1038/nprot.2014.143

40. Luk KC, Kehm V, Carroll J, Zhang B, O'Brien P, Trojanowski JQ, et al. Pathological α-Synuclein Transmission Initiates Parkinson-like Neurodegeneration in Nontransgenic Mice. Science (80-). 2012;338(6109):949. Available from: http://science.sciencemag.org/content/338/6109/949.abstract

41. Mao X, Ou MT, Karuppagounder SS, Kam T-I, Yin X, Xiong Y, et al. Pathological α-synuclein transmission initiated by binding lymphocyte-activation gene 3. Science. 2016 Sep 30;353(6307):aah3374. Available from: https://pubmed.ncbi.nlm.nih.gov/27708076

42. Kam T-I, Mao X, Park H, Chou S-C, Karuppagounder SS, Umanah GE, et al. Poly(ADP-ribose) drives pathologic α-synuclein neurodegeneration in Parkinson's disease. Science. 2018 Nov 2;362(6414):eaat8407. Available from: https://pubmed.ncbi.nlm.nih.gov/30385548

43. Hallam RD, Buchner-Duby B, Stykel MG, Coackley CL, Ryan SD. Intracellular Accumulation of α-Synuclein Aggregates Promotes S-Nitrosylation of MAP1A Leading to Decreased NMDAR-Evoked Calcium Influx and Loss of Mature Synaptic Spines. J Neurosci. 2022 Dec 14;42(50):9473 LP – 9487. Available from: http://www.jneurosci.org/content/42/50/9473.abstract

44. Bhullar KS, Lagarón NO, McGowan EM, Parmar I, Jha A, Hubbard BP, et al. Kinase-targeted cancer therapies: progress, challenges and future directions. Mol Cancer. 2018 Feb 19;17(1):48. Available from: https://pubmed.ncbi.nlm.nih.gov/29455673

45. Gouda NA, Elkamhawy A, Cho J. Emerging Therapeutic Strategies for Parkinson's

896   Disease and Future Prospects: A 2021 Update. Vol. 10, Biomedicines. 2022.

897   46.   L. BE, Aaron M, D. SK, S. BK, Mastooreh C, E. MT, et al. Alpha-Synuclein Expression
898   Restricts RNA Viral Infections in the Brain. J Virol. 2022 May 2;90(6):2767–82.
899   Available from: https://doi.org/10.1128/JVI.02949-15

900   47.   Allen Reish HE, Standaert DG. Role of α-synuclein in inducing innate and adaptive
901   immunity in Parkinson disease. J Parkinsons Dis. 2015;5(1):1–19. Available from:
902   https://pubmed.ncbi.nlm.nih.gov/25588354

903   48.   Rousseaux MWC, de Haro M, Lasagna-Reeves CA, De Maio A, Park J, Jafar-Nejad P, et
904   al. TRIM28 regulates the nuclear accumulation and toxicity of both alpha-synuclein and
905   tau. Ackerman SL, editor. Elife. 2016;5:e19809. Available from:
906   https://doi.org/10.7554/eLife.19809

907   49.   Rousseaux MWC, Revelli J-P, Vázquez-Vélez GE, Kim J-Y, Craigen E, Gonzales K, et
908   al. Depleting Trim28 in adult mice is well tolerated and reduces levels of α-synuclein and
909   tau. Ackerman SL, editor. Elife. 2018;7:e36768. Available from:
910   https://doi.org/10.7554/eLife.36768

911   50.   Karczewski KJ, Francioli LC, Tiao G, Cummings BB, Alföldi J, Wang Q, et al. The
912   mutational constraint spectrum quantified from variation in 141,456 humans. Nature.
913   2020;581(7809):434–43. Available from: https://doi.org/10.1038/s41586-020-2308-7

914   51.   Sorrentino ZA, Vijayaraghavan N, Gorion K-M, Riffe CJ, Strang KH, Caldwell J, et al.
915   Physiological C-terminal truncation of α-synuclein potentiates the prion-like formation of
916   pathological inclusions. J Biol Chem. 2018;293(49):18914–32. Available from:
917   https://www.sciencedirect.com/science/article/pii/S0021925820311297

918   52.   Ma L, Yang C, Zhang X, Li Y, Wang S, Zheng L, et al. C-terminal truncation exacerbates
919   the aggregation and cytotoxicity of α-Synuclein: A vicious cycle in Parkinson's disease.
920   Biochim Biophys Acta - Mol Basis Dis. 2018;1864(12):3714–25. Available from:
921   https://www.sciencedirect.com/science/article/pii/S0925443918303806

922   53.   Tofaris GK, Reitböck PG, Humby T, Lambourne SL, O'Connell M, Ghetti B, et al.
923   Pathological Changes in Dopaminergic Nerve Cells of the Substantia Nigra and Olfactory
924   Bulb in Mice Transgenic for Truncated Human α-Synuclein(1–120): Implications for
925   Lewy Body Disorders. J Neurosci. 2006 Apr 12;26(15):3942 LP – 3950. Available from:
926   http://www.jneurosci.org/content/26/15/3942.abstract

927   54.   Moors TE, Maat CA, Niedieker D, Mona D, Petersen D, Timmermans-Huisman E, et al.
928   The subcellular arrangement of alpha-synuclein proteoforms in the Parkinson's disease
929   brain as revealed by multicolor STED microscopy. Acta Neuropathol. 2021;142(3):423–
930   48. Available from: https://doi.org/10.1007/s00401-021-02329-9

931   55.   Zhang M, Zhang L, Geng A, Li X, Zhou Y, Xu L, et al. CDK14 inhibition reduces
932   mammary stem cell activity and suppresses triple negative breast cancer progression. Cell
933   Rep. 2022;40(11):111331. Available from:
934   https://www.sciencedirect.com/science/article/pii/S2211124722011597

935

936

937

Figures

939 **Figure 1. Loss of Cdk14 ameliorates grip strength impairment and α-Syn pathology in PFF-**

940 **injected mice.** (A) Mouse α-Syn PFFs were injected unilaterally into the striatum by stereotactic

941 injection in 6-month-old mice. (B) Loss of forelimb grip strength at 6 months post α-Syn PFF-

942 treatment in WT mice, but not in *Cdk14*$^{+/-}$ or *Cdk14*$^{-/-}$ mice. Mean + SEM, two-way ANOVA,

943 Bonferroni *post hoc,* n: 9-10. (C) α-Syn PFF-injection increased the load of pS129 α-Syn-positive

944 cells (depicted without and with hematoxylin counterstaining, 50 μm scale bars) in the injected

945 hemisphere (ipsilateral, IL; injection site indicated by *). Densities of pS129 α-Syn-positive cells

946 are represented in heat maps as hues of red at 3 rostrocaudal levels (relative to bregma: +0.98 mm,

947 +0.26 mm, and -1.34 mm) with dark shades of red correlating to high cell densities (injection sites

948 marked by asterisks). Amounts of pS129 α-Syn-positive cells in all brain regions (averaged in IL

949 and contralateral to the injection, CL), the somatomotor cortex and the striatum at +0.26 mm

950 relative to bregma of PFF-injected *Cdk14*$^{+/-}$ and *Cdk14*$^{-/-}$ mice were lower relative to their wildtype

951 (WT) counterparts. Mean + SEM, two-way ANOVA, Bonferroni *post hoc* comparisons*,* n: 3-6.

952 (D) PFF injection reduces the tyrosine hydroxylase (TH)-positive fiber density IL in comparison

953 to the non-injected hemisphere (CL) to a similar degree in WT, *Cdk14*$^{+/-}$ and *Cdk14*$^{-/-}$ mice at

954 +0.26 mm relative to bregma (200 μm scale bar). Mean + SEM, two-way ANOVA, Bonferroni

955 *post hoc* comparisons, n: 3-7.

956

957 **Figure 2. Primary cortical neurons lacking Cdk14 exhibit decreased spreading of seed-**

958 **competent α-Syn**

959 (A) Paradigm for passaging PFF-transduced WT, *Cdk14*$^{+/-}$, and *Cdk14*$^{-/-}$ primary culture media to

960 WT, naïve cultures. Media from 21 DIV cultures transduced with PFFs for 14 days were collected,

961   filtered, and added to naïve cultures at 7 DIV. Media-treated cultures were then fixed and analyzed

962   for fluorescent pS129 α-Syn signal. (B) Conditioned media from *Cdk14*^{+/-} and *Cdk14*^{-/-} neurons

963   induce less α-Syn pathology (indicated by pS129 α-Syn-positive area) in naïve WT neurons

964   compared to WT conditioned media (50 µm scale bars). Mean + SEM, two-way ANOVA, Holm-

965   Šídák post hoc comparisons, n=4.

966

967   **Figure 3. Genetic reduction of Cdk14 attenuates pS129 α-Syn in human neurons.**

968   Immunoblots illustrating elevated amounts of pS129 α-Syn in the RIPA buffer-soluble protein

969   fraction of hiPSC-derived *SNCA* A53T human neurons (in comparison to isogenic corrected

970   neurons [Corr]) which is reduced by CRISPR/Cas9-mediated knockdown of *CDK14* (targeted

971   against *CDK14* exon 3 (E3) and 8 (E8), NT non-targeting control). Mean + SEM, one-way

972   ANOVA, Tukey *post hoc* comparisons, n=3-4.

973

974   **Figure 4. Pharmacological inhibition of CDK14 reduces α-Syn protein burden in human and**

975   **rodent neurons.** (A) Dose-dependent reduction of α-Syn in hESC-derived human neurons is

976   detected by ELISA-quantification after 6 days of CDK14 inhibitor FMF-04-159-2 treatment. Mean

977   + SEM, one-way ANOVA, Bonferroni *post hoc* comparisons, n=3. (B) Human α-Syn PFFs applied

978   to rat cortical neurons for 5 days increase the amounts of α-Syn and CDK14 in the insoluble protein

979   fraction (Urea buffer-soluble) compared to untreated (UT) and α-Syn monomers (Mono)-treated

980   neurons, as shown by immunoblots, which were reduced by the application of 100 nM of the

981   CDK14 inhibitor. Mean + SEM, two-way ANOVA, Holm-Šídák *post hoc* comparisons, n=3.

982

983 **Figure 5. Inhibition of Cdk14 decreases human α-Syn protein in mice expressing A53T**

984 ***SNCA.*** (A) Intracerebroventricular (ICV) administration strategy for the CDK14 inhibitor FMF-

985 04-159-2 at 0.35 mg/kg/day for 28 days in 4-month-old *PAC α-Syn*^{A53T} *TG* mice. (B) Immunoblots

986 with protein isolated from the brain of FMF-04-159-2-treated *PAC α-Syn*^{A53T} *TG* mice visualize

987 the reduction of α-Syn in the TSS buffer-soluble, Cdk14 in the TXS buffer and SDS buffer-soluble

988 and C-terminally truncated (CTT) α-Syn (arrowhead at high exposure (high exp.)) in the TSS

989 buffer- and TXS buffer-soluble protein fraction in comparison to vehicle-treated mice. Mean +

990 SEM, unpaired student's *t* test, n=6.

991

992

993

994

995

996

997

998

999

1000

1001

1002

1003

1004

1005

39

Fig. 1
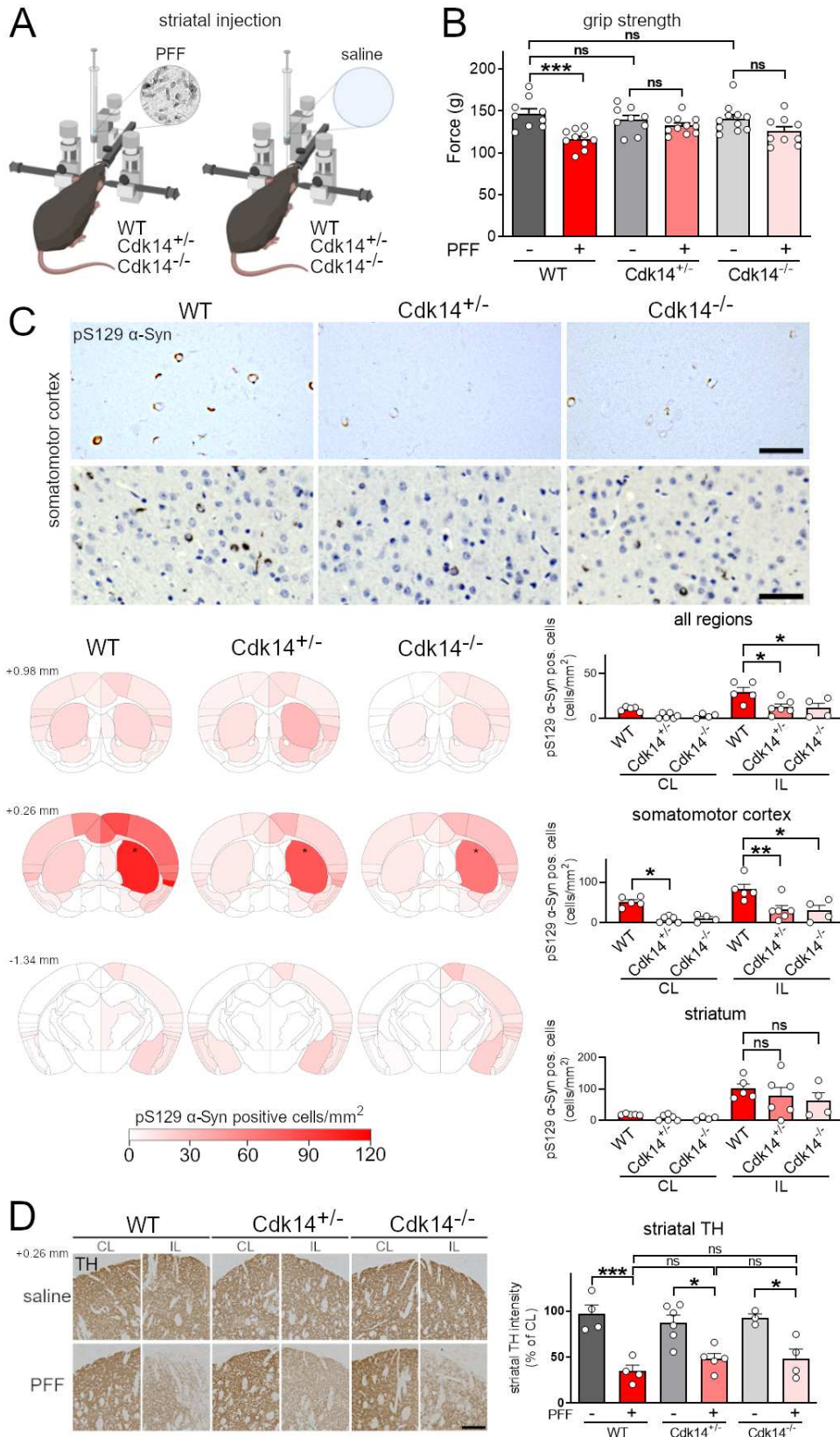
1008
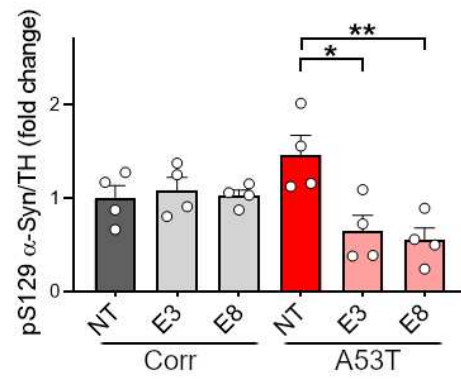
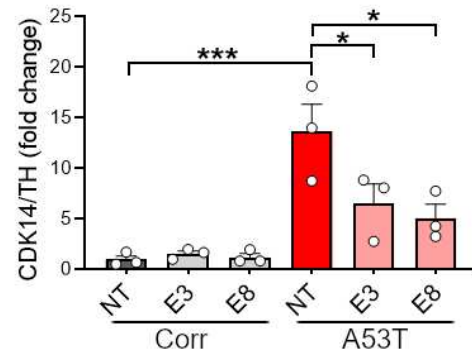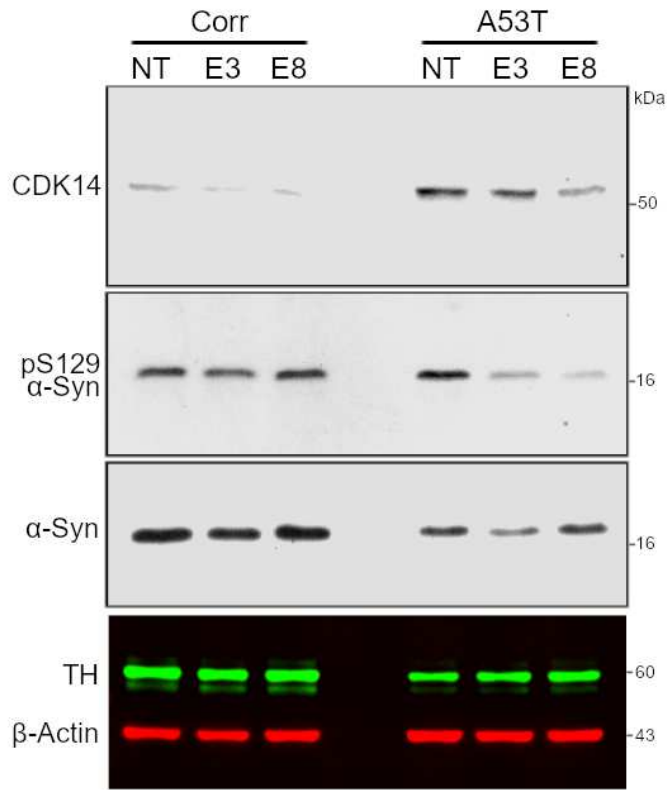1009 **Fig. 2**
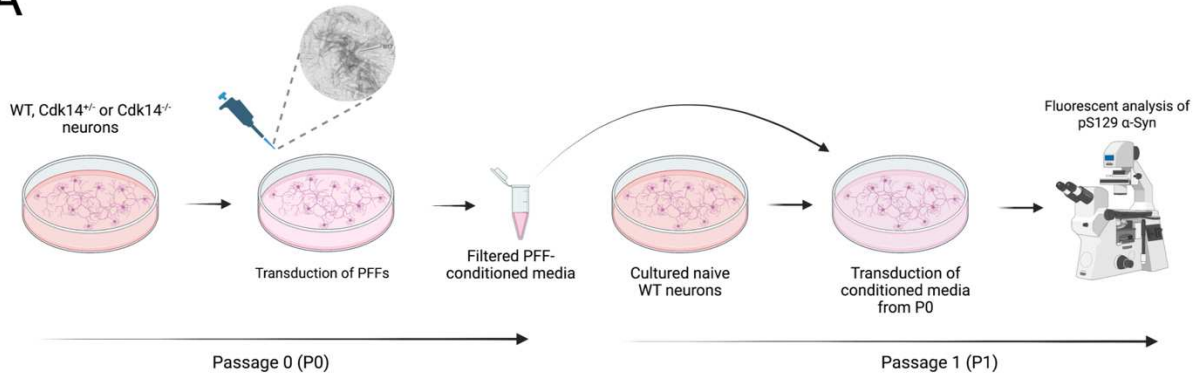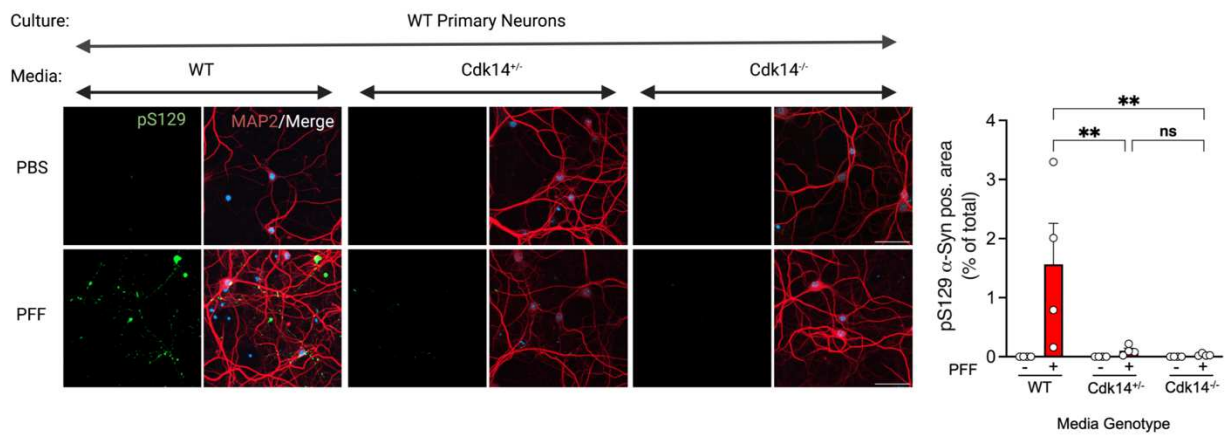
1010

1011

1012

1013

1014

1015

1016

1017

1018

41

Fig. 3

1020

1021

1022

1023

1024

1025

1026

1027

1028

1029

1030

1031

42

1032 **Fig. 4**
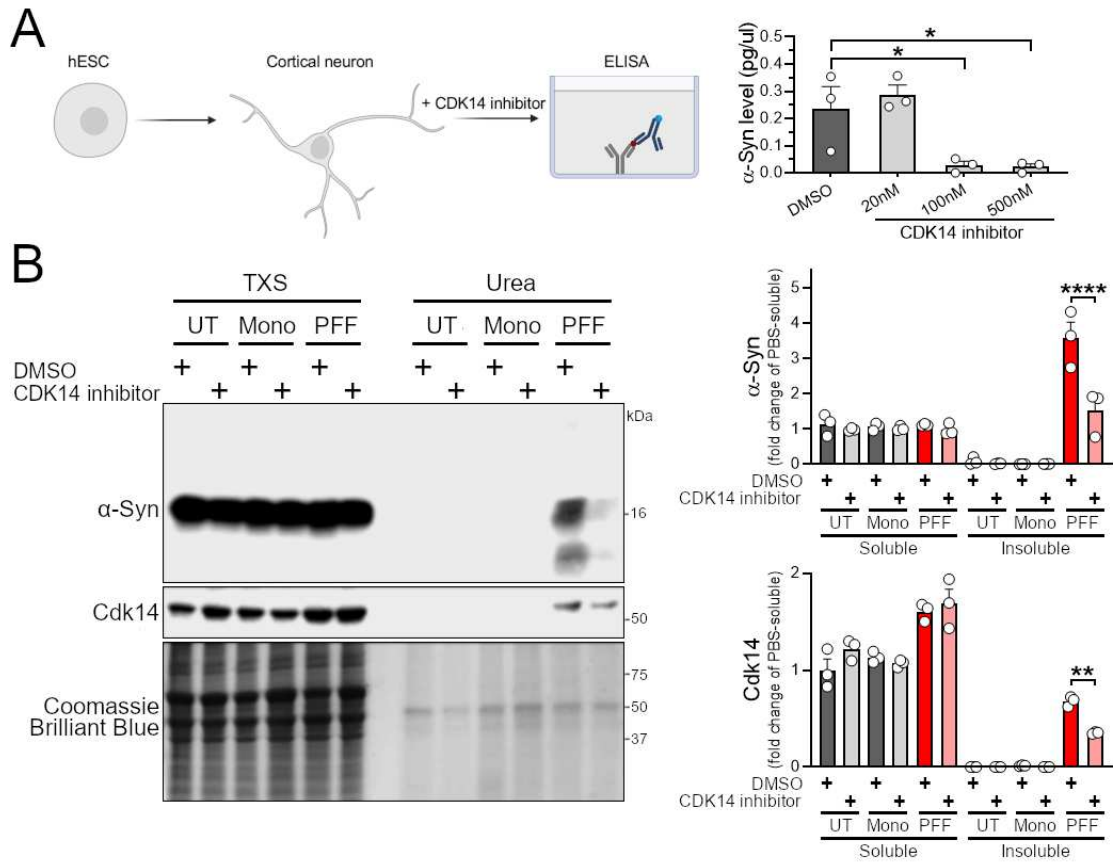

1033

43

Fig. 5

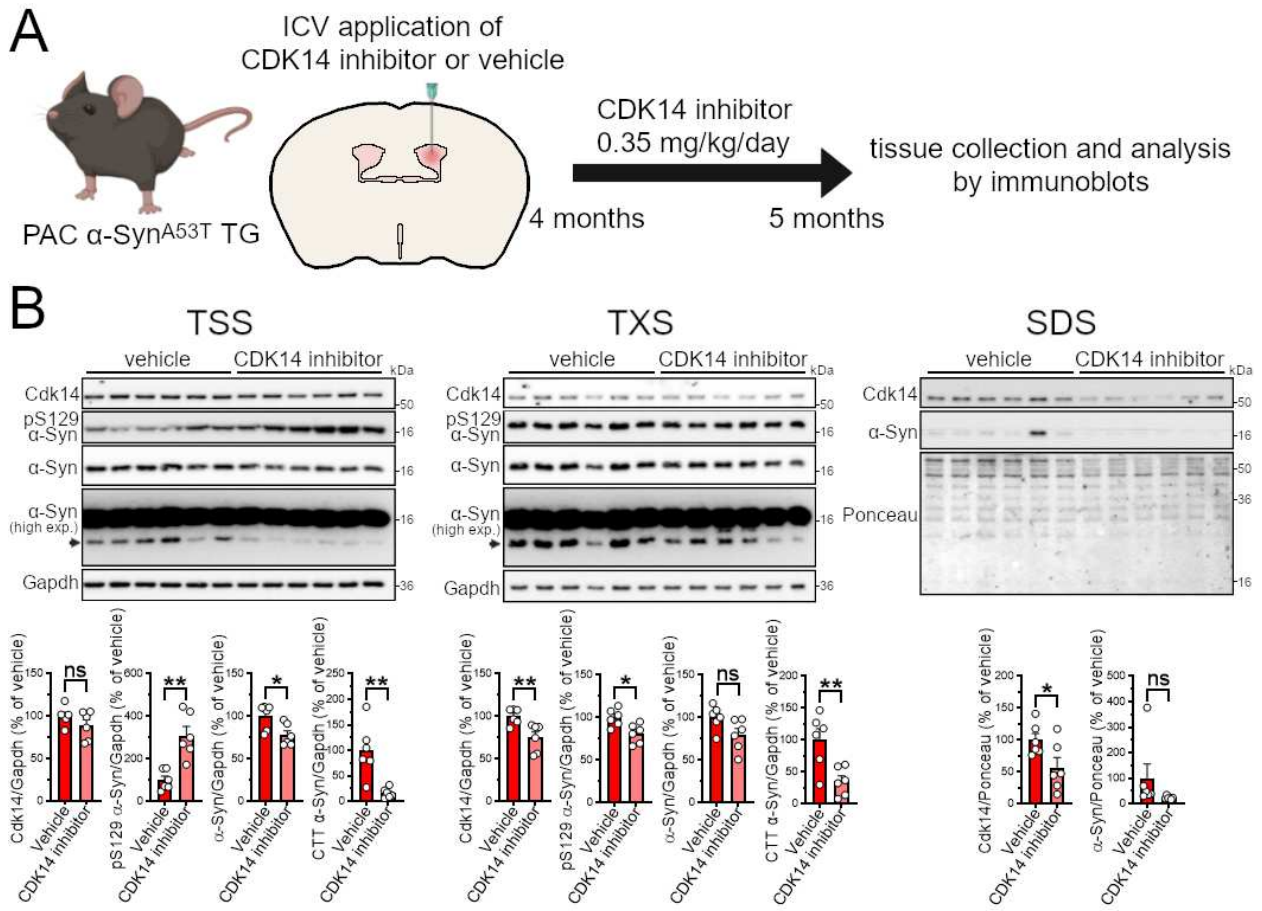# Supplementary Files

This is a list of supplementary files associated with this preprint. Click to download.

- CDK1418072023Supp.pdf